Hindawi
Journal of Nanomaterials
Volume 2019, Article ID 8457383, 18 pages
https://doi.org/10.1155/2019/8457383

*Review Article*

# A Short Review on Verwey Transition in Nanostructured $Fe_3O_4$ Materials

**Murtaza Bohra**,[1] **Nishit Agarwal**,[1] **and Vidyadhar Singh**[2]

[1]*Mahindra École Centrale, College of Engineering, Hyderabad, 500043 Telangana, India*
[2]*Department of Physics, Jai Prakash University, Chapra, 841301 Bihar, India*

Correspondence should be addressed to Murtaza Bohra; murtazaphy@gmail.com and Vidyadhar Singh; vsraj47@gmail.com

Received 5 August 2018; Revised 22 November 2018; Accepted 17 December 2018; Published 25 March 2019

Academic Editor: P. Davide Cozzoli



Verwey transition (VT) of $Fe_3O_4$ has been extensively investigated as this results in sharp changes in its physical properties. Exploitation of VT for potential applications in spin/charge transport, multiferroicity, exchange bias, and spin Seebeck effect-based devices has attracted researchers recently. Although hundreds of reports have been published, the origin of VT is still debatable. Besides, not only the size effects have a significant impact on VT in $Fe_3O_4$, even the conditions of synthesis of $Fe_3O_4$ nanostructures mostly affect the changes in VT. Here, we review not only the effects of scaling but also the growth conditions of the $Fe_3O_4$ nanostructures on the VT and their novel applications in spintronics and nanotechnology.

## 1. Introduction

The metal-insulator transition also known as Verwey transition (VT) in strongly correlated magnetite ($Fe_3O_4$) system is vital for its potential applications in nanoelectronics, spintronics, and mottoronix [1]. From a scientific point of view, the VT provides information to understand the extraordinary crystal lattice (regarding the freezing-in fluctuating lattice) and electronic structure (charge, spin, and orbital) order of $Fe_3O_4$ [2, 3]. However, owing to the many competing degrees of freedom, the close energetic proximity of the different phases (presence of twining) often obscures the exact nature of the VT as they are probed in thermal equilibrium. Technologically, the resistive switching behaviour in $Fe_3O_4$ thin films at VT shows high potential for alternative memory applications, such as gate voltage-driven resistive switching in field-effect transistors [4]. On the other hand, the large change observed in magnetoresistance and spin Seebeck coefficient around VT makes it useful for sensors and solid-state energy conversion devices [5–7]. Thus, ever since then $Fe_3O_4$ and in particular the VT has been an object of extensive research and great debate. Although experimental and theoretical progress has recently been made on $Fe_3O_4$, the origin of the VT is still under discussion.

$Fe_3O_4$ is a cubic ferrimagnetic oxide with the highest magnetization $M = 4.2\,\mu_B$ below Curie temperature, $T_C = 858$ K. Band structure calculations predict half-metallic (-100% spin polarization) character of $Fe_3O_4$ with room temperature conductivity, $\sigma = 200\ (\Omega{\cdot}\mathrm{cm})^{-1}$ [8, 9]. Stoichiometric $Fe_3O_4$ shows VT wherein first-order structural phase transformation occurs around 124 K ($T_V$) [10]. In the low-temperature phase, $Fe_3O_4$ is an insulator, has a monoclinic structure connected to the charge ordering, and exhibits an orbital order on the $Fe^{2+}$ sites [11]. Also, it was found that localized electrons are shared between three Fe ions on octahedral *B*-lattice sites which can be termed as trimerons [8]. This transition also has manifestations in resistivity, heat capacity, magnetization, and many other properties [3]. Therefore, VT, which has a potential in cutting-edge technologies, provides an external tuning competency of the properties by changing the temperature. Despite the tremendous progress in nanostructured $Fe_3O_4$, it is still an open question how the VT changes in the nanoregime. The most critical difficulty in the size-dependent characterization of VT is the synthesis of uniform and stoichiometric nanostructured $Fe_3O_4$ because VT is reported to be extremely sensitive to the oxygen stoichiometry [12]. The size of nanostructure having the VT varies in different reports, as stoichiometry

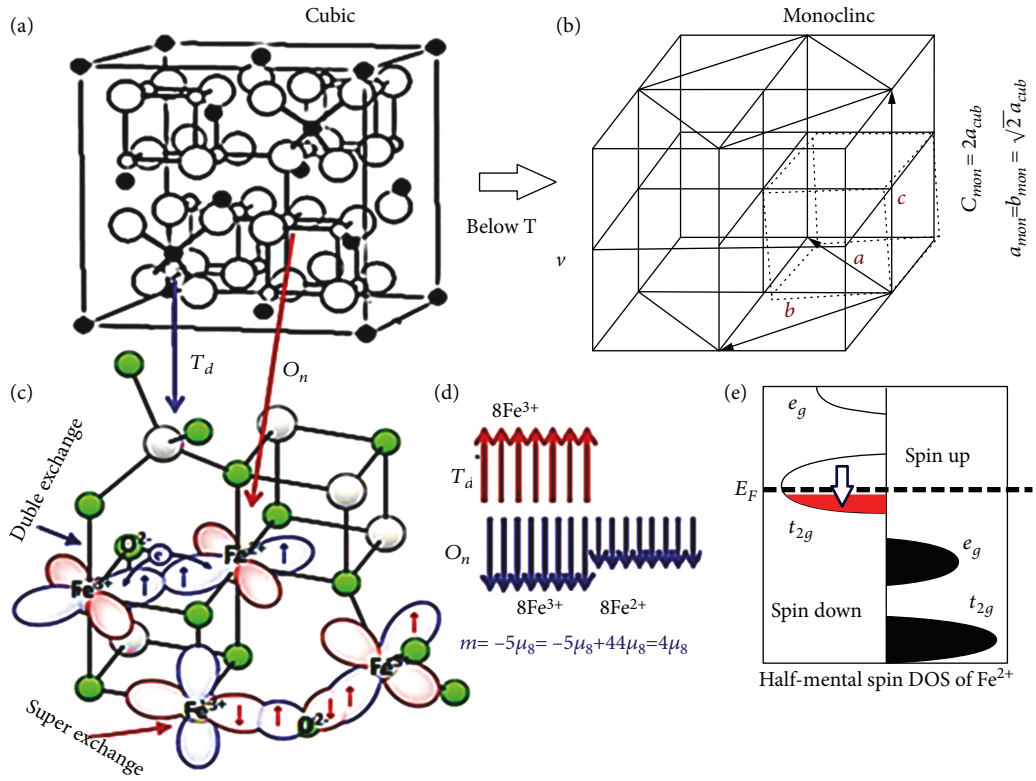


FIGURE 1: Cubic inverse spinel structure of $Fe_3O_4$ with tetrahedral and octahedral sites above $T_V$ (a) and distorted monoclinic crystal structure below the $T_V$ (b). The double and superexchange interaction mechanisms (c) [13]. Sketch of the localized structure of the spins at tetrahedral and octahedral sites (d). The density of states occupied by electrons of $Fe^{+2}$ ions at octahedral sites (e).

commonly depends on growth conditions. Furthermore, at the nanoscale, the VT is difficult to technically observe because diffraction methods suffer from severe peak broadening due to the small crystallite size [9]. The occurrence of superparamagnetism hampers the observation in magnetometry, and measurements of the conductivity are difficult to interpret in the case of ensembles of nanoparticles, since the path of the electric current may simply change [9].

Thus, the understanding of VT in nanostructured $Fe_3O_4$ is the main focus of this review. Here, we shall discuss the best growth methods and characterization techniques which are being currently employed to investigate nanostructured $Fe_3O_4$ material and their potential applications. Before presenting the results on nanostructured $Fe_3O_4$, some basic properties of $Fe_3O_4$ shall be summarized.

## 2. Material Properties of $Fe_3O_4$

*2.1. Crystalline Properties.* $Fe_3O_4$ possesses an inverse spinel structure $AB_2O_4$ (space group $Fd3m$; $a = 8.39$ Å) (Figure 1(a)), wherein oxygen anions form a cubic face-centred (fcc) lattice, and the large interstices between $O^{2-}$ are partially occupied by iron cations. Tetrahedral $A$ positions are occupied by $Fe^{3+}$ cations, while octahedral $B$ positions are equally occupied by $Fe^{3+}$ and $Fe^{2+}$ cations ($[Fe_{Td}{}^{3+}]_A[Fe_{Oh}{}^{3+}Fe_{Oh}{}^{2+}]_BO_4$) [8, 9]. In $Fe_3O_4$, ferrimagnetism exists through two main mechanisms, as shown in Figure 1(c). The first is the antiferromagnetic superexchange interactions between the $Fe_{Oh}{}^{3+}$ and $Fe_{Td}{}^{3+}$ cations through the $O^{2-}$ anions [13, 14]. The spin-up $5d$ electrons in the $Fe_{Oh}{}^{3+}$ couple with the overlapping $2p$ orbitals in the $O^{2-}$ making them spin down. The other $2p$ electron is thus spin-up which makes the $Fe_{Oh}{}^{3+}5d$ electrons spin down. Thus, $Fe_{Oh}{}^{3+}$ and $Fe_{Oh}{}^{3+}$ are antiparallel and cancel out each other's unpaired spin magnetic moments. The second factor is related to the double-exchange interaction [15] in which the spin-down electron can only hop from $Fe_{Oh}{}^{2+}$ to $Fe_{Oh}{}^{3+}$ if the majority spins are the same. Hence, they are coupled and aligned parallel. Therefore, all the $Fe^{2+}$ cations contribute to the magnetic moment while all $Fe^{3+}$ cations cancel each other out, resulting net magnetic moment $(9 - 5 = 4)\ \mu_B$ (see Figure 1(d)). Because of the strong antiferromagnetic A-B superexchange interaction, A-A and B-B superexchange interactions become ferromagnetic resulting in the ferrimagnetic structure of $Fe_3O_4$. The extra electron of $Fe_{Oh}{}^{2+}$ ions is transferred to the empty orbitals of $Fe_{Oh}{}^{3+}$ by displacing electrons from the intervening $O^{2-}$ ions in a double-exchange process: $Fe_{Oh}{}^{2+}$ to $O^{2-}$ and $O^{2-}$ to $Fe_{Oh}{}^{3+}$. The room temperature conductivity of $Fe_3O_4$ is, thus, attributed to this hopping of electrons ($Fe^{2+} \rightleftharpoons Fe^{3+} + e^-$) at octahedral $B$-sites. The extra electron of the $Fe^{2+}$ ion occupies the minority $t_{2g}$ band, which is the only band located at Fermi level $E_f$, giving rise to half-metallicity as predicted by band structure calculation, shown in a simplistic form in Figure 1(e) [8, 9].

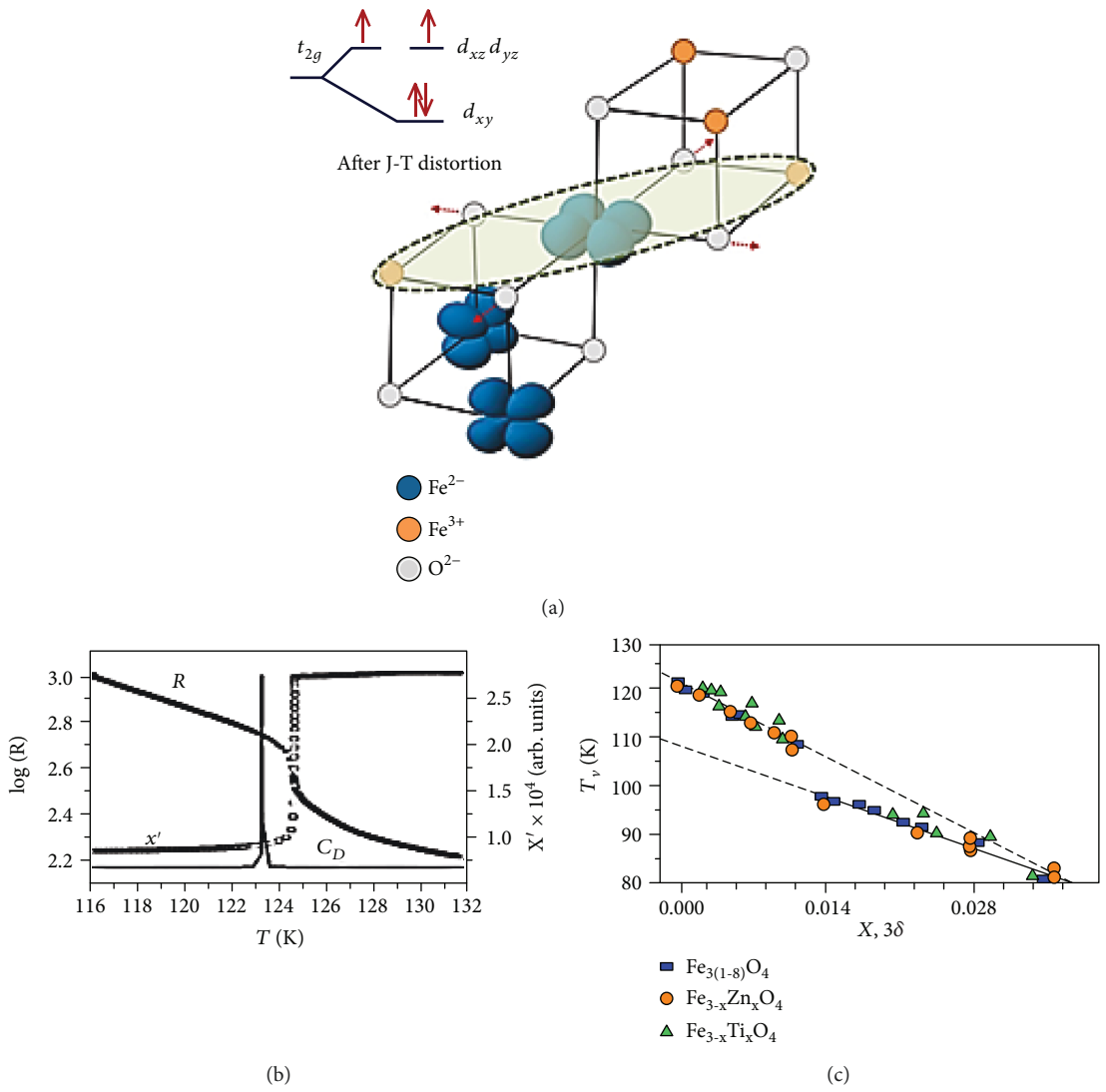


FIGURE 2: Energy separation due to Jahn-Teller distortion (up) and depiction of trimeron concept in single $Fe^{+2}O_6$ octahedra (down) (a) [8]. Changes in magnetic susceptibility, resistance, and specific heat at $T_V$ (b) [10, 17]. For clarity, the temperature scale for $R$ and $\chi'$ was shifted concerning the true temperature scale. With an increasing number of vacancies or doped atoms, the VT shifts to low temperatures (c) [18].

*2.2. Verwey Transition.* Upon cooling of $Fe_3O_4$ below the $T_V$, the electron hopping between $Fe^{2+}$ and $Fe^{3+}$ ions freezes, and the combination of 2+ and 3+ species then arranges themselves in a regular pattern without moving (charge ordering). In this nonconducting state, the stagnant $Fe^{2+}$ ions are Jahn-Teller (J-T) active [8]; this means that the extra electron in $Fe^{2+}$ has a choice between occupying any one of the three available half-filled orbitals $d_{xy}$ or the two $d_{xz/yz}$, as they all have the same energy (see the top of Figure 2(a)). Electrons prefer to occupy the orbit with the least energy. To break this choice, an effective energy separation between $d_{xy}$ and $d_{yz}/d_{zx}$ is created in the four Fe–O bonds (depicted by red arrows in the bottom of Figure 2(a)) in the $xy$ plane that are elongated or contracted. The negative value of $\Delta t_{2g}$ signifies that the energy of $d_{xy}$ is lower than that of $d_{yz}/d_{zx}$, that is, tetragonal distorted $Fe^{2+}O_6$ octahedra with elongated Fe–O bonds in the $xy$ plane. On top of this, an additional structural distortion in which B-site Fe-Fe distances within linear $Fe^{3+}$-$Fe^{2+}$-$Fe^{3+}$ units (depicted by the grey ellipsoid in the bottom of Figure 2(a)) is anomalously shortened showing that electrons are not fully localized as $Fe^{2+}$ states but are instead spread over the three sites resulting in highly structured three-site polarons defined as a single *trimeron* [8]. The J-T distortion in $Fe^{2+}O_6$ octahedra mentioned earlier directly couples to the neighbouring $Fe^{3+}O_6$ octahedra constituting the trimerons, although they are J-T inactive in the first approximation. Due to trimeron formation, distances from $Fe^{2+}$ states to their two B-site neighbours in the local orbital ordering plane are anomalously shortened. The cumulative effect of this trimeron shortening penetrates throughout the crystal in the various trimeron locations to significantly perturb the cubic $Fe_3O_4$ structure to the complex overall distortion. The cubic spinel- $(a = b = c)$ type structure of $Fe_3O_4$ distorts to a monoclinic superstructure with Cc space group symmetry $(a = b \neq c)$ $(\sqrt{2}, \sqrt{2}, 2)$, as

shown in Figure 1(b). This structural transformation was first found by Verwey in 1939 and was named after him [16, 17]. The charge, orbital, and trimeron orders of $Fe_3O_4$ stand out perhaps as the most complex electron-ordered ground state known.

Because of this structural transformation in $Fe_3O_4$, many physical properties (specific heat, magnetic susceptibility, and resistance) show abrupt change around $T_V$ [3] (see Figure 2(b)). It has been reported that several factors can affect VT of bulk $Fe_3O_4$ negatively, such as oxygen off-stoichiometry and cation substitution. The $T_V$ gradually decreases from 124 to 80 K and finally vanishes completely with increasing oxygen off-stoichiometry or cation substitution ($Ti^{2+}$, $Zn^{2+}$, etc.) (see Figure 2(c)) [18].

Even after an intense research, there still exist two major schools of interpretation: the first one interprets the VT as a transition driven by charge/orbital ordering and the second one exploits the mechanism of a lattice distortion-driven charge ordering leading to metal-insulator behaviour.

## 3. Observation of Verwey Transition in Various $Fe_3O_4$ Nanostructures

Recently, a lot of work has been carried out to study the effect of various nanostructured $Fe_3O_4$ morphologies on VT, which include single crystals, epitaxial and polycrystalline thin films, particles, arrays of colloidal nanocrystals, heterostructures, and also in the form of nanocontacts. The eventual utilization of these morphologies is to develop novel VT-based devices, and this is a critical issue for further investigations.

*3.1. Nanoparticles (*1 nm < Particle Size < 100 nm*).* The recent advancement in the synthesis of uniform and size-controllable $Fe_3O_4$ nanocrystals has enabled the size-dependent physical property characterization and their applications [21]. Recently, Lee et al. [20] have successfully synthesized stoichiometric and uniform-sized $Fe_3O_4$ nanocrystals with sizes ranging from 5 to 100 nm. These nanocrystals show the VT in the conductance, magnetization, and heat capacity measurements (see Figures 3(a)–3(c)). The VT is generally masked in magnetization data of superparamagnetic nanocrystals below the blocking temperature; therefore, it was reassured that the heat capacity of nanocrystals shows a lambda-like anomaly similar to the single crystal $Fe_3O_4$, confirming a truly thermodynamic transition. $^{57}Fe$ nuclear magnetic resonance (NMR) of $Fe_3O_4$ nanocrystals (7 nm-7 $\mu$m) was also measured [19]. The line width of NMR spectra changes drastically around 120 K (see Figure 3(d)), showing microscopic evidence of the Verwey transition. The inset shows the NMR spectral intensity for one of the representative samples (25 nm) obtained at temperatures around the $T_V$. In the region above the transition temperature, the line width of the spectrum increases and the spin-spin relaxation time decreases as the nanocrystal size decreases. The line width broadening indicates the significant deformation of magnetic structure and reduction of charge order compared to bulk crystals, even when the structural distortion is unobservable. The VT is weakly size-dependent (see Figure 3(e)) and gets suppressed in nanocrystals smaller than 20 nm before completely disappearing for a size less than 6 nm, which is a clear yet highly interesting indication of a size effect of this well-known phenomenon.

*3.2. Nanocrystalline Thin Films (*1 nm < Grain Size < 100 nm*).* Considering the spintronic applications concerning magnetoresistance (MR) that depends on the spin polarization of the materials being used, an in-depth study of the growth of nanocrystalline $Fe_3O_4$ thin films is of interest. A relatively large low-field MR (-6% at 300 K to -10.0% at 200 K at the field of 5 kOe) was indeed found in nanocrystalline films [22]; however, in most cases, large MR could only be obtained at a high field and especially at low temperatures. The MR response in $Fe_3O_4$ seems to be very sensitive to the preparation conditions, and the reason for low or inconsistent MR response could be because of the nonstoichiometry grain boundaries and surface spin arrangement. In literature, nanocrystalline $Fe_3O_4$ thin films have been grown by a range of deposition techniques, such as evaporation, sputtering, molecular beam epitaxy, and pulsed laser deposition (PLD) [23–25].

Previously, the author has worked extensively on oxide films, and we consider that the PLD [26–28] is the most suitable technique for stoichiometric growth of complex oxides. The deposition of $Fe_3O_4$ has been performed in a reducing atmosphere (under the vacuum of $1 \times 10^{-5}$ mbar and substrate temperature, $T_S$: RT-850°C) from the $\alpha$-$Fe_2O_3$ target on an amorphous quartz substrate [26]. This regime can produce $Fe_3O_4$ in a limited $T_S$ window of 350-500°C (see Figure 4(a): Fe/O phase diagram). These films were followed by two different annealing processes, namely, (1) vacuum annealing and (2) wet $H_2$ annealing, in that the wet $H_2$ annealing only produces single-phase $Fe_3O_4$ films with grain sizes ranging 30-60 nm. The normalized $M$ vs. $T$ curve shows noticeable VT (see Figure 4(b)) which is a useful indicator for the stoichiometry of the samples, except for a higher $T_S$ film showing a broad transition due to slight Fe/O off-stoichiometry.

The electric transport properties of the nanocrystalline $Fe_3O_4$ thin films are not well defined as compared to the magnetic properties, particularly the absence of VT (see Figure 4(b)). To understand this contradictory behaviour, we plotted $M/M$ (300 K) vs. $T$ curves at different fields for one of the representative samples ($T_S = 500$°C), as shown in Figure 5(a). We see that the magnitude of the drop in magnetizations at VT has severely reduced from 40% to 0.4% with the increasing field from 0.5 to 20 kOe [27]. This raises a question if this drop in magnetization is due to a change of the magnetic moment of $Fe_3O_4$ or is it just a manifestation of the increased anisotropy. The $M$-$H$ loops (inset) support our arguments that the nonsaturation of magnetization at high fields and coercivity have increased significantly below VT. We fitted the high-field part of $M$-$H$ loops to the approach to saturation formula, $4\pi M = Q[1 - (H*/H)^{1/2}]$, where $Q$ is the magnetization at the infinite field and $H^*$ is related to the magnetocrystalline anisotropy [27]. The $Q$ vs. $T$ curve (Figure 5(b)) does not show any drop in magnetizations around VT as was seen in Figure 5(a) for low fields. We

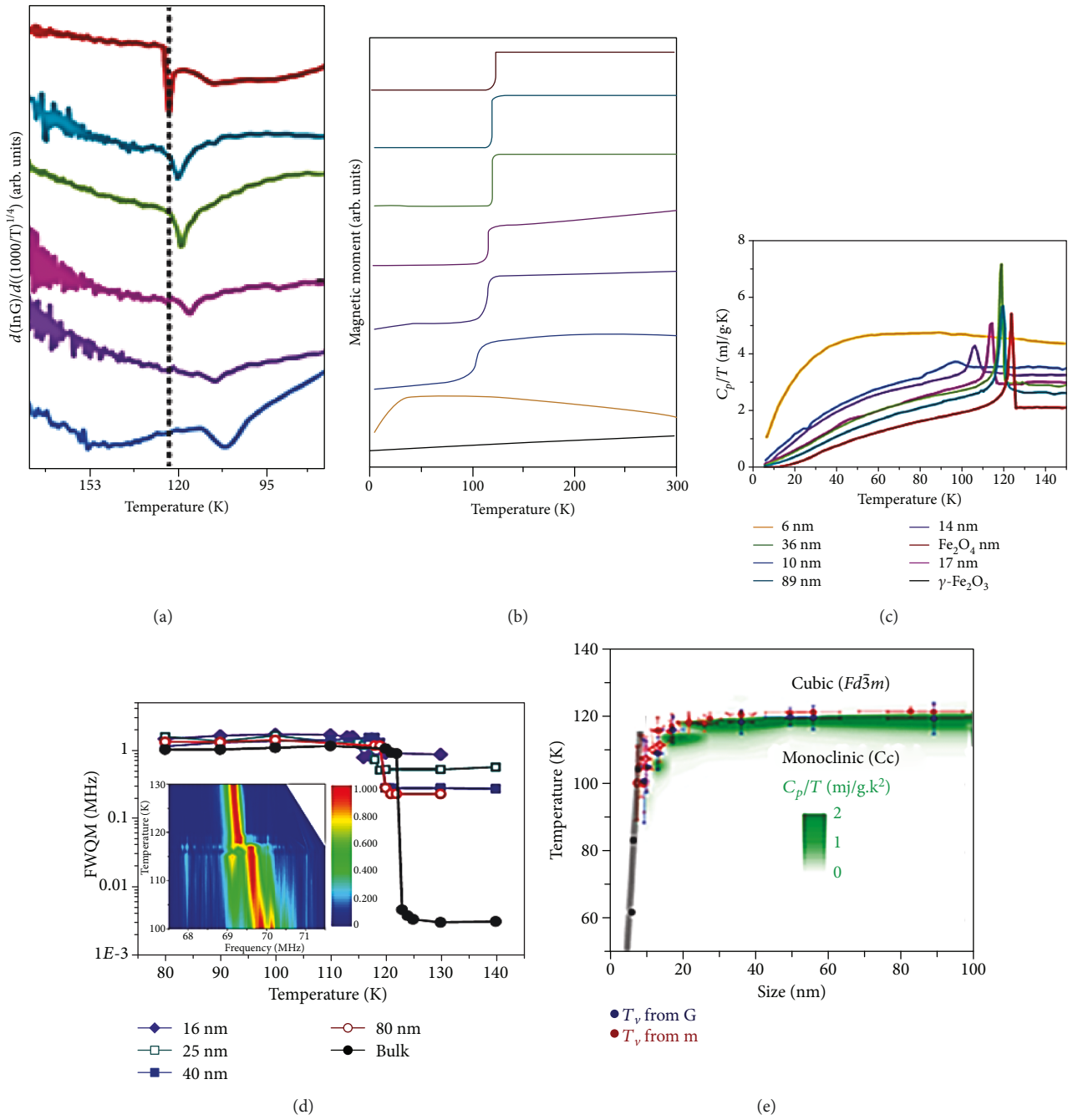


FIGURE 3: Size-dependent characterization of the VT: temperature dependence of the first derivative of conductance (a), magnetization data measured at 100 Oe (b), and total heat capacity divided by temperature (c). The full width at quarter maximum (FWQM) of the Fe NMR spectra versus temperature [19]. The inset shows the Fe NMR spectral intensity of the 25 nm sample obtained at temperatures around $T_V$ (d). Size dependence of VT from combined data (e) [20].

can conclude that the intrinsic saturation magnetic moment does not show any drop while cooling across VT, and whatever drop in magnetization we observed in Figure 5(a), it is just because of inadequate saturation field and there is nothing to do with any magnetic interaction change. This transition can also happen even if there is no structural transition but if there is a change in anisotropy. We now argue that charge order is triggered by the structural transition and it has nothing to do with magnetic ordering, as discussed by us elsewhere [28]. So the absence of VT in electronic transport may have a different origin like grain boundary volume, and defects/vacancies induced intergranular strain in nanocrystalline $Fe_3O_4$ films that suppress the resistivity change caused during VT [28].

Another interesting feature comes from large magnetocaloric effect observed in these nanocrystalline $Fe_3O_4$ films around VT, as shown in Figure 5(c). The fitting of $M$-$H$ loops in Maxwell equations [29], $\delta S_M = \int_{H_i}^{H_f} (\partial M/\partial T) dH$,

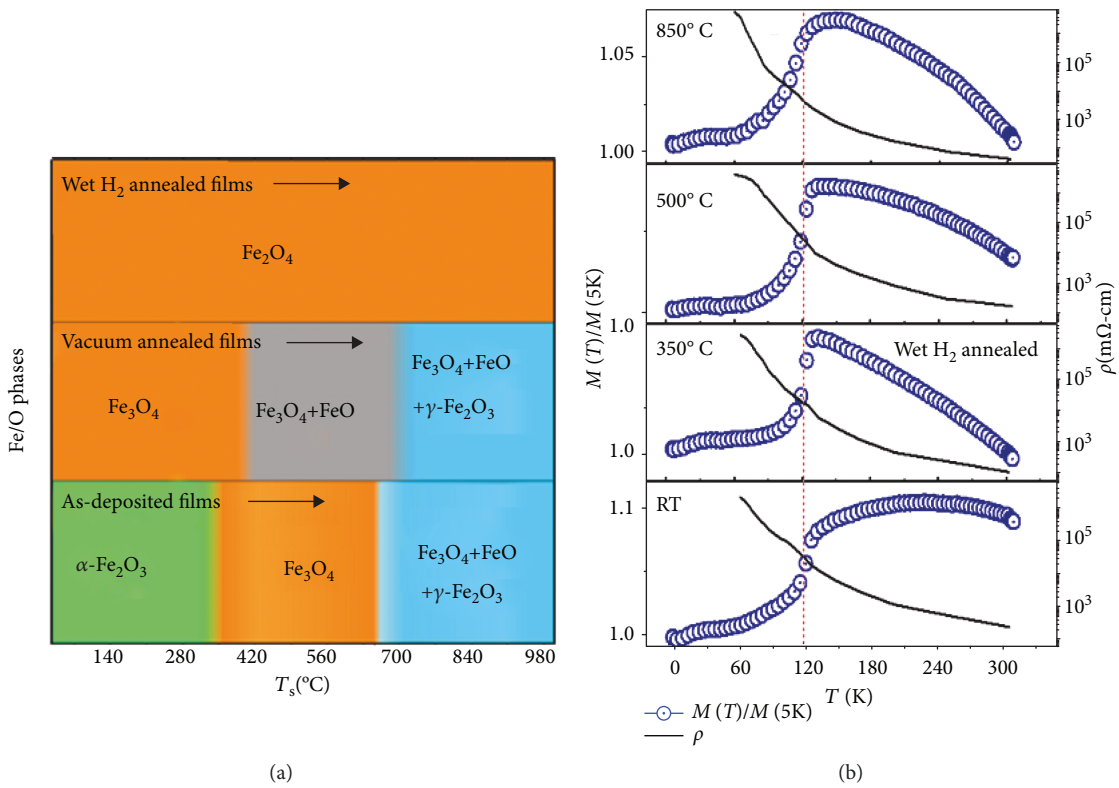


FIGURE 4: Various Fe/O phases at different $T_S$ before and after reduction treatments (a), $M(T)/M$ (5 K) (at the fixed field of 5 kOe) and $\rho$ vs. $T$ curves for wet $H_2$ annealed films at different $T_S$ (b) [26].

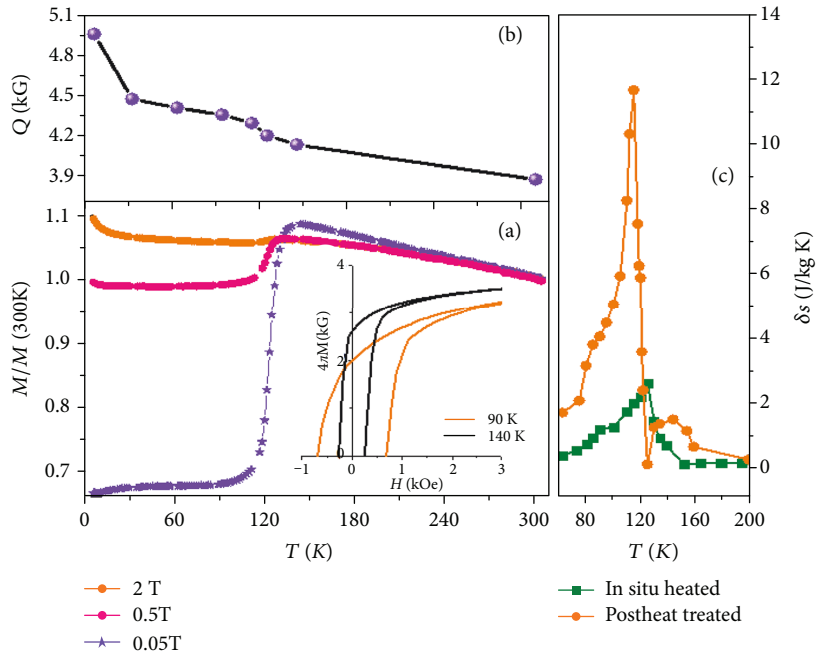


FIGURE 5: $M$ vs. $T$ curves under various fixed fields (a). The inset shows $M$-$H$ loops below and above VT. The $Q$ vs. $T$ curves deduced from Chikazumi's formula (b) [27] and $\delta S$ vs. $T$ curves for in situ and ex situ annealed $Fe_3O_4$ films (c) [29].

yield large positive entropy change $\delta S = 2\text{-}12$ J/kg K at VT under the field of 10 kOe. The magnitude of $\delta S$ depends upon the detail microstructures of nanocrystalline films produced by different thermal treatments. This result is significant for cooler on-chip devices for next-generation nano-/microelectromechanical systems (NEMS/MEMS).

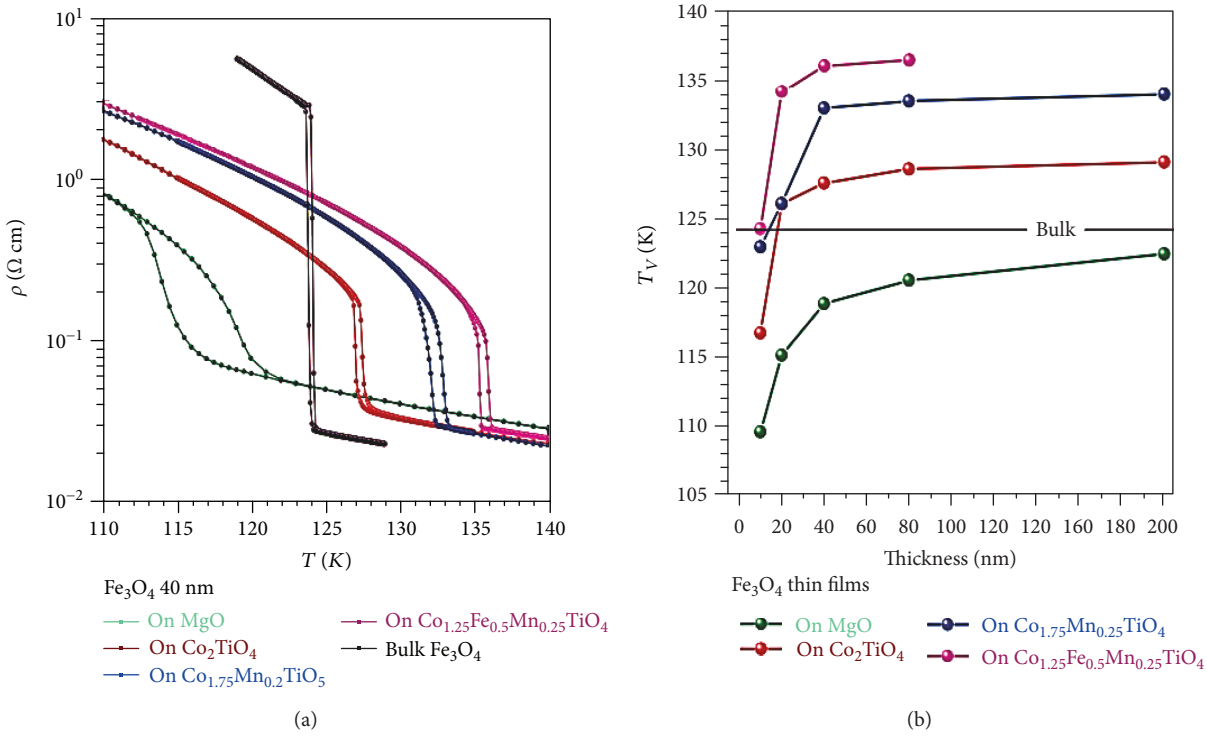


FIGURE 6: $\rho$ vs. $T$ curves for 40 nm epitaxial $Fe_3O_4$ films grown on MgO (001), $Co_2TiO_4$ (001), $Co_{1.75}Mn_{0.25}TiO_4$ (001), and $Co_{1.25}Fe_{0.5}Mn_{0.25}TiO_4$ (001) substrates along with single-crystal $Fe_3O_4$ (a). Corresponding $T_V$ vs. thickness curves (b) [30].

*3.3. Epitaxial Films (*1 nm < Nanothick < 200 nm*).* Despite the remarkable amount of work devoted in preparing $Fe_3O_4$ thin films in the last two decades, the VT even in epitaxial thin films is extremely broad and occurs at substantially lower temperatures as compared to the high-quality bulk single crystals. A systematic study on the influence of oxygen stoichiometry on epitaxial $Fe_3O_4$ films found that even for the optimal oxygen composition, the transition remains broad [22]. The study also discovered that the microstructure of the films has an important role; particularly, a larger domain size distribution results in a broader transition and a small domain size gives lower transition temperatures. The transition itself is still first order as it shows hysteresis, and there are indications that each domain has its transition temperature. Various substrates have been used in the literature to grow epitaxial $Fe_3O_4$ thin films, e.g., MgO, $MgAl_2O_4$, $Al_2O_3$, $SrTiO_3$, and $BaTiO_3$ [30]. These studies suggest that the larger the lattice mismatch, the broader the transition and the lower the average transition temperature.

Recently, Liu et al. [30] succeeded in making a particular class of spinel substrates that allows the growth of $Fe_3O_4$ thin films with the VT as sharp as in bulk. The key principle was to obtain sufficiently large domain sizes of $Fe_3O_4$ thin films with small domain size distribution. Figure 6(a) shows $\rho$ vs. $T$ curves of 40 nm thick $Fe_3O_4$ (001) films grown on MgO and spinel substrates ($Co_2TiO_4$, $Co_{1.75}Mn_{0.25}TiO_4$, and $Co_{1.25}Fe_{0.5}Mn_{0.25}TiO_4$), along with bulk $Fe_3O_4$ single crystal. We can see that the bulk sample has a sharp VT at 124 K, whereas the film on MgO shows the typical broad transition at lower temperatures. In contrast, the thin films grown on the spinel substrates all show a very sharp transition, almost as sharp as the bulk with a hysteresis value of 0.7 K. The most exciting feature is that now the transition temperatures of thin films grown on spinel substrates (127 K on $Co_2TiO_4$ (lattice mismatch +0.66%), 133 K on $Co_{1.75}Mn_{0.25}TiO_4$ (+0.98%), and 136 K on $Co_{1.25}Fe_{0.5}Mn_{0.25}TiO_4$ (+1.11%)) are even higher than those of the bulk [31–35]. Figure 6(b) shows that $T_V$ gradually increases with the film thickness and, again, that it is larger for the spinel substrates with the larger lattice constant mismatch between the film and the substrate. Although films with the thicknesses of 5 nm and less do not show a VT, we can see a well-defined transition for films when they are 10 nm or thicker. Thus, using tensile strain, one can increase the transition temperature into considerably higher values than bulk. The occurrence of the VT in the highly anisotropic strained films raises a new question on the intricacies of the interplay between the charge and orbital degrees of freedom of the Fe ions in $Fe_3O_4$, adding another aspect to the elusiveness of this quantum material.

The anisotropic magnetoresistance (AMR) of high-quality epitaxial $Fe_3O_4$ films on MgO (100) and $Al_2O_3$ (0001) substrates [36] was investigated in charge-ordering state, as shown in Figure 7(a). It was found that the Verwey transition contains two processes, a fast charge-ordering process and a continuous formation of trimeron process. In the $Fe_3O_4$ (100) film, the twofold AMR at 104 K < 116 K comes from the uniaxial magnetic anisotropy, whereas the fourfold AMR at $T$ = 104 K can be ascribed to the in-plane trimerons (Figure 7(b)). However, AMR in the $Fe_3O_4$ (111) film maintains twofold symmetry (Figure 7(c)). By comparing the AMR below $T_V$ between two oriented films, it shows the maxima when the trimerons are parallel to the magnetic

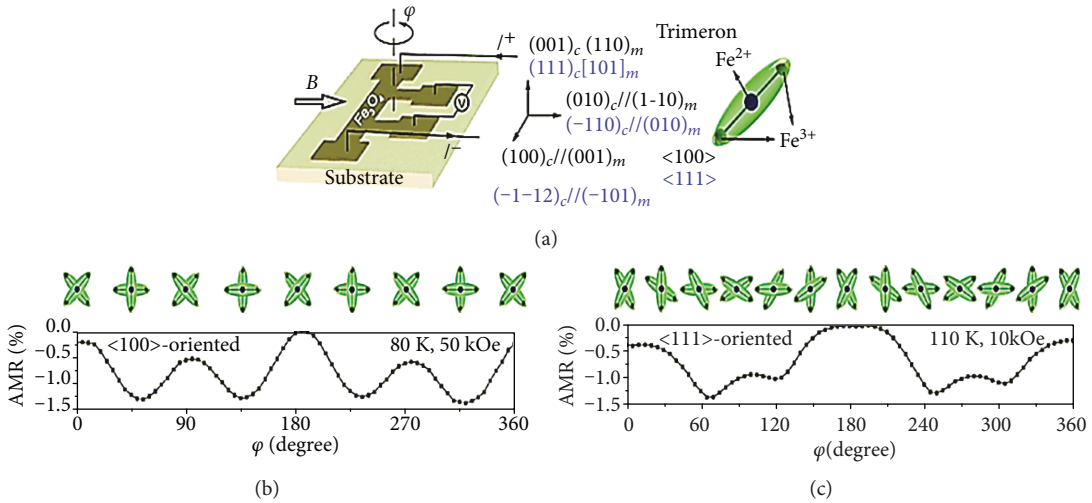


FIGURE 7: Sketch map of the sample, magnetic field, and current arrangement in the left corner (a). The structure of trimeron is shown in the right corner (a). AMR at 80 K and 50 kOe of $Fe_3O_4$ (100) film and the in-plane trimeron distribution at the corresponding angle (b). AMR at 110 K and 10 kOe of $Fe_3O_4$ (111) film and the in-plane trimeron distribution at the corresponding angle (c) [36].

field. A uniaxial magnetic anisotropy might appear in the trimeron, and the easy axis is along the trimeron. Thus, in-plane trimerons play an important role in the complex AMR behaviour below the $T_V$.

*3.4. Other Nanostructured $Fe_3O_4$ Geometries.* While a lot of work has been done in thin film form, little is known about the potential use of $Fe_3O_4$ for device applications in nanoparticle morphology. Also, the VT is very sensitive to stoichiometry, and it is hardly observed in superparamagnetic length scale; an alternate approach to optimize the stoichiometry is to tailor the shape of the particles, since anisotropy plays a crucial role in deciding the magnetic characteristics of the magnetic nanocrystals. Recently, Mitra et al. [1] investigated the VT in shape-controlled small amine-coated $Fe_3O_4$ nanoparticles (6–14 nm). The VT of $Fe_3O_4$ near 120 K is seen in octahedral particles (Figure 8(a)), but it is not observed in their spherical particles (Figure 8(b)) in the FC- (field cooled-) ZFC (zero field cooled) measurements. The facets of octahedral particles consist of energetically most stable {111} planes which are protected against surface oxidation. The surface anisotropy is substantially reduced since the flat surface of octahedron has fewer broken bonds and oxygen vacancies. A lower concentration of defects and almost no oxidized layer at the surface provide a better stoichiometry to octahedral particles, which is the cause of the VT in octahedral nanoparticles.

Unfortunately, the crystal quality of spherical nanoparticles suffers from surface spin disorder and uncompensated bonds; epitaxial $Fe_3O_4$ nanorods with well-defined magnetic anisotropy are very promising as building blocks in spintronic devices. Chandra et al. [37] demonstrated the epitaxial growth of highly oriented $Fe_3O_4$ nanorods on $SrTiO_3$ substrates by hydrothermal synthesis, as depicted in Figure 8(c). The epitaxial nanorods show biaxial magnetic anisotropy with an order of magnitude difference between the anisotropy field values of the easy and hard axes along with sharp VT. The interplay of epitaxy and enhanced magnetic anisotropy at room temperature, concerning randomly oriented $Fe_3O_4$ powder, and the nanorods are useful materials for magnetic data storage. Differently, $Fe_3O_4$ nanocubes [38] synthesized by the oxidation of $Fe_{1-x}O/Fe_{3-\delta}O_4$ core-shell nanocubes (see in Figure 8(d)) show a kink at 110 K in the ZFC curve which can be attributed to the VT; however, it is not that much sharp as observed in nanorods and octahedral particles of $Fe_3O_4$.

## 4. Applications

*4.1. Multiferroic Properties.* In addition to all its acclaimed fame, $Fe_3O_4$ is also probably one of the first multiferroics, which shows the ferroelectric effect (FE) in its insulating state below VT [39–48]. However, the microscopic nature of the FE in $Fe_3O_4$ is still a matter of debate. Probably, it is related to the coexistence of bond-centred and charge-centred charge ordering. In the proposed structural and charge pattern, besides the site-centred charge ordering, one also notices the alternation of the formal $Fe^{2+}$ and $Fe^{3+}$ valence states and strong modulation of the Fe-Fe distances (the bond lengths). In the structure shown in Figure 9(a) [49], one sees that, e.g., along the Fe chains running in the (110) direction (in cubic setting), i.e., in the *xy* chains, there is an alternation of $Fe^{2+}$ and $Fe^{3+}$ (open and filled circles), but simultaneously there is an alternation of short and long Fe-Fe bonds. This direction corresponds to the monoclinic b-direction, in which the polarization is observed. In this framework, each of such (110) mixed bond- and site-centred charge-ordering chains gives a nonzero contribution to the electrical polarization.

Firmly, the proof for the existence of FE order (as shown in Figure 9(b)) in 150 nm thick $Fe_3O_4$ films synthesized by pulsed laser deposition and magnetron sputtering on Nb-doped $SrTiO_3$ substrates has been investigated recently [50]. The appearance of ferroelectric order below 38 K was

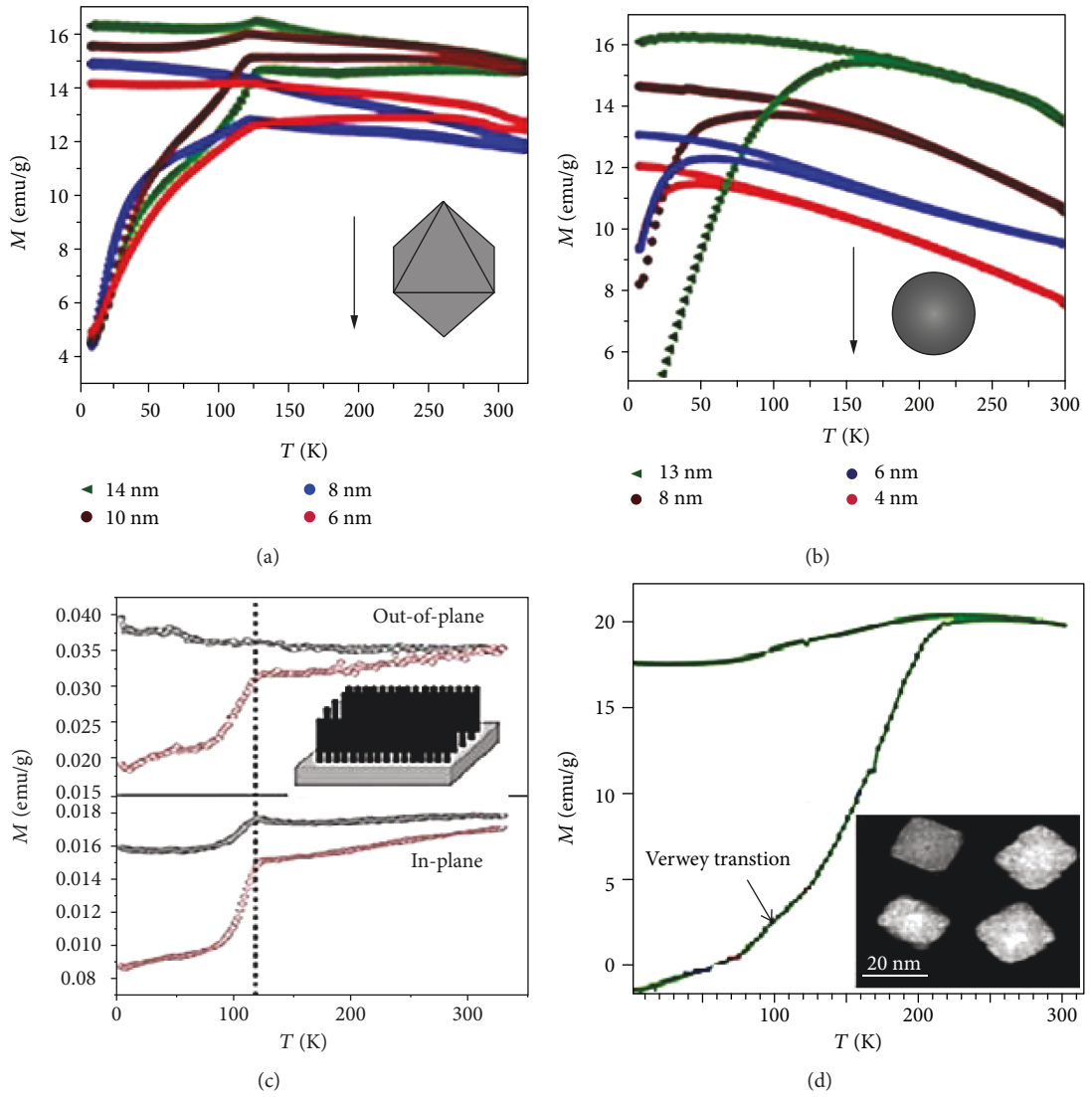


Figure 8: FC and ZFC magnetizations for different sizes of spherical and octahedral $Fe_3O_4$ nanoparticles (a, b) [1]. FC and ZFC magnetization of epitaxial $Fe_3O_4$ nanorods (along in- and out-of-plane directions) (c) and nanocubes (d) [37]. Insets (a–d) show the surface morphology of nanostructured $Fe_3O_4$ materials [38].

explained by the existence of spontaneous electric polarization in the noncentrosymmetric monoclinic Cc structure, which arises from an alternation of charge states and bond lengths [51, 52]. However, it is surprising that the electric polarization does not already develop at the VT. This is because in between 40 K and $T_V$, the electric polarization is suppressed by relaxation processes due to electron tunnelling and electron hopping processes [53], glassy polar degrees of freedom [54], or thermally activated structural processes [55]. Since the easy-axis direction is generally stabilized by the film-substrate strain, it would be easier to observe a ferroelectric polarization in thin films than in bulk. Indeed, the polarization values measured in $Fe_3O_4$ films tend to be larger than in single crystals. This scenario explains the close relation between magnetoelectric effects and relaxation processes observed both in the electric and magnetic susceptibilities. In contrast to conventional relaxor ferroelectrics [56], the relaxor behaviour in $Fe_3O_4$ is not driven by chemical heterogeneity but by the dynamical structural disorder.

Conventionally, the multiferroics are single-phase materials with the coexistence of ferromagnetism, ferroelectricity, or ferroelasticity, which can result in novel functionalities. Because of advancement of the thin-film growth techniques and computational capabilities, the coupling in multiferroics that was predicted in 1894 has developed rapidly [57, 58]. In the class of single-phase multiferroic materials, magnetism occurs independently from ferroelectricity. Some multiferroic heterostructures have been produced by compound ferromagnetics ($Fe_3O_4$) with ferroelectrics $BaTiO_3$ [59], $Pb(Mg_{1/3}Nb_{2/3})O_3$-$PbTiO_3$(PMN-PT) [60], $PdZr_xTi_{1-x}O_3$ (PZT) [61], $BiFeO_3$ [62], $HoMnO_3$, and $YMnO_3$ [63]. These multiferroic heterostructures show the strong interfacial magnetoelectric effects [64–69], which can be used in

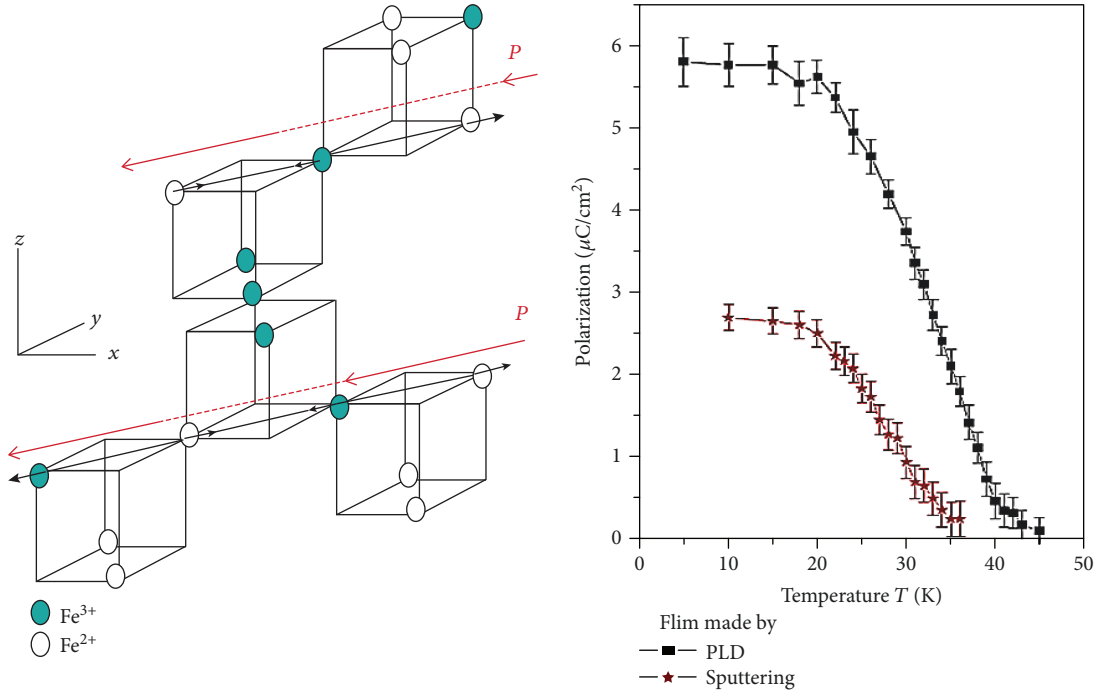


FIGURE 9: Sketch of the possible origin of ferroelectricity in $Fe_3O_4$ and emphasis on the Fe chains running in the (110) direction of $Fe_3O_4$ []. In the *xy* chains, there is an alternation of $Fe^{2+}$ and $Fe^{3+}$ ions (open and filled circles). Concurrently, there is an alternation of short and long Fe-Fe bonds; shifts of Fe ions are shown by black arrows. The resulting polarization is indicated by the red arrows (a) [49]. Electric saturation polarization of the $Fe_3O_4$ films made by pulsed laser deposition and sputtering (b) [50].

multifunctional spintronic, nanoelectronic, and optoelectronic devices.

Electric-field-controlled magnetism and VT in highly correlated $Fe_3O_4$ materials have generated great interest recently both scientifically and technologically [51]. Ferroelastic strain control of VT was observed in epitaxial $Fe_3O_4$ thin films grown on PMN-PT (011) substrate [4], as shown in four-point geometry (Figure 10(a)). Through ferroelastic control of lattice strain, the $T_V$ shot up by 8 K, evidenced by large changes in resistivity once the sample is poled with a DC field of 10 kV/cm (inset Figure 10(a)). Thus, electrical modulation of in-plane epitaxial strain is a far more effective way to manipulate VT than a pure volume change argument. On the other hand, epitaxial $Fe_3O_4$ films incorporated into a gated device structure [51] (Figure 10(b)) demonstrate the ability to control the VT with static electric fields. The $T_V$ increases for both polarities of the electric field, indicating that the effect is not driven by changes in carrier concentration. The energetics of induced electric polarization and strain within the $Fe_3O_4$ film provides a possible explanation for this behaviour.

Another example of magnetoelectric coupling is the magnetic properties of $Fe_3O_4/BaTiO_3$ heterostructures which observe remarkable changes (as shown in Figure 11) at various structural phase transitions of $BaTiO_3$ substrate [70]. Upon tetragonal to orthorhombic transition (T to O), the lattice parameter of $BaTiO_3$ dramatically decreases, which induces compressive strain in the $Fe_3O_4$ thin film. This increased strain anisotropy leads to an abrupt increase of in-plane magnetization, coercivity, and remanent magnetization of $Fe_3O_4$ (Figures 11(b) and 11(c)) [70]. While in transition from orthorhombic to rhombohedral (O to R), the lattice parameter of $BaTiO_3$ now dramatically increases, resulting in a decrease of the compressive strain, which leads to an opposite effect on magnetic properties of $Fe_3O_4$ (Figures 11(b) and 11(c)). The $Fe_3O_4$ (001) film, which has a negative magnetostriction coefficient, is under compressive stress when it is in contact with $BaTiO_3$. With the decrease of temperature, the lattice mismatch between $Fe_3O_4$ and $BaTiO_3$ increases. These temperature-driven structural transformations of $BaTiO_3$ induce various anisotropies that cause magnetic properties to change, in a way similar to the VT, however at elevated temperatures.

The quantitative understanding of converse magnetoelectric effects, i.e., the variation of the magnetization as a function of an applied electric field in extrinsic multiferroic hybrids, is a key prerequisite for the development of future spintronic devices. The strain-mediated converse magnetoelectric effect in $Fe_3O_4/BaTiO_3$ heterostructures was also realized at room temperature [34]. This demonstrates that the electric-field-induced changes of the magnetic state in the $Fe_3O_4$ thin film can be well described by the presence of two different ferroelastic domains in the $BaTiO_3$ substrate, resulting in two differently strained regions in the $Fe_3O_4$ film with different magnetic properties. The two-region model allows predicting the converse magnetoelectric effects in multiferroic hybrid structures consisting of ferromagnetic thin films on ferroelastic substrates.

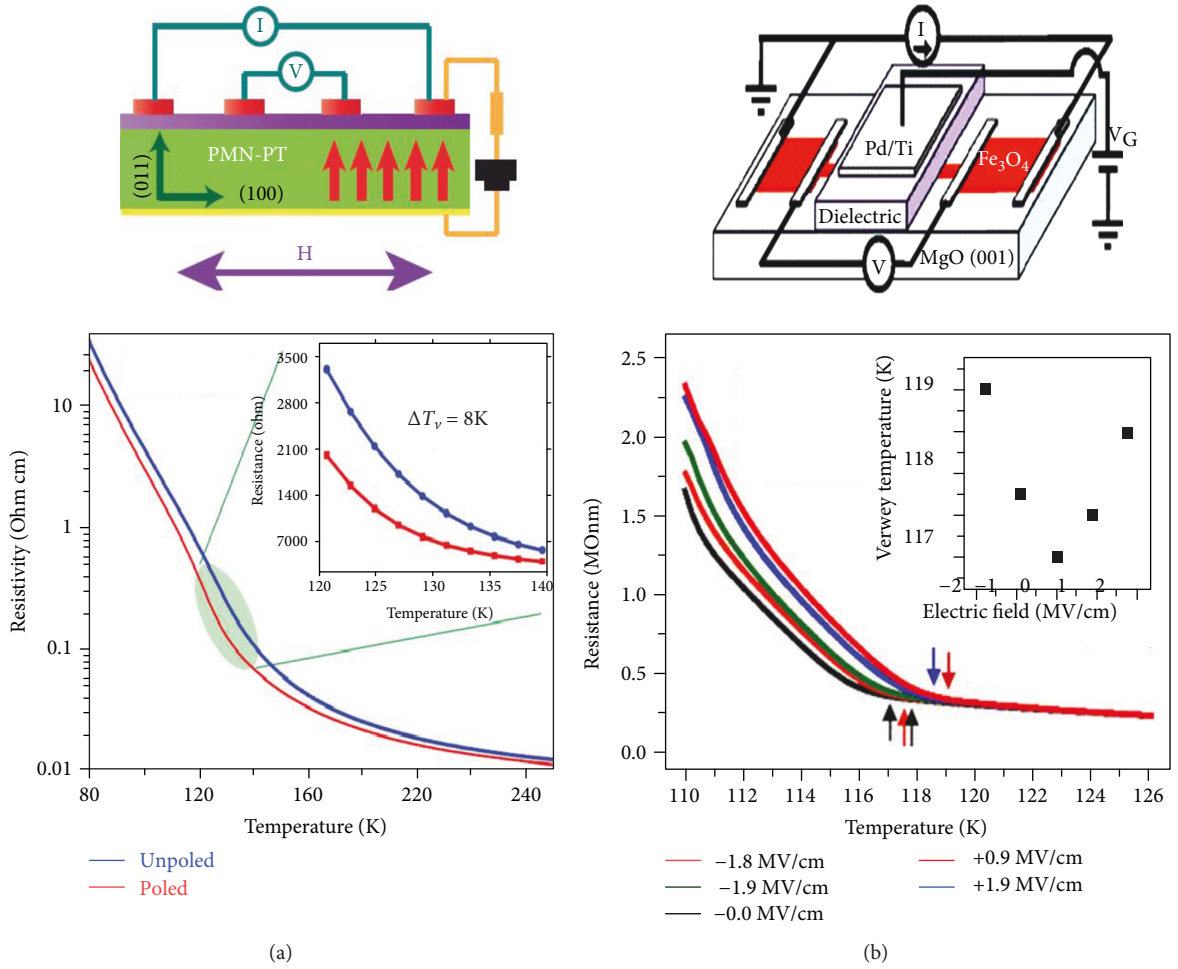


FIGURE 10: Schematics of four-point resistance measurement for $Fe_3O_4$/PMN-PT structure and ferroelastic strain state dependence of resistivity as a function of temperature (a) [4]. Electrical gating of $Fe_3O_4$ where the dielectric layer consists of PMMA (900 nm)/$Al_2O_3$ (50 nm)/MgO (10 nm). Temperature dependence of resistance for applied electric fields of +1.8 MV/cm (blue), +0.9 MV/cm (orange), 0 MV/cm (black), −0.9 MV/cm (green), and −1.8 MV/cm (red). The arrows show $T_V$ for each electric field, which is summarized in the inset (b) [51].

Digital memory comes with the ability to switch between distinct electronic and magnetic phases with a control voltage. Small changes in structure and charge density near a transition between competing phases can tip the balance among them, leading to large changes in electronic and magnetic properties. Devices based on this principle can be both fast and energy efficient [71], overcome some of the intrinsic limitations in conventional field-effect transistors [72], and also provide new functionalities [73–75]. While these properties point to a pathway for creating novel functionalities, reversible and nonvolatile switching between different phases using strain has been unexplored. In nonvolatile switching, the electronic/magnetic states that are realized remain in a stable remnant state after the control voltage has been switched off.

*4.2. Spin Seebeck Effect.* The spin Seebeck effect (SSE) refers to the generation of a spin voltage caused by a temperature gradient in a ferromagnet, which enables the thermal injection of spin currents from the ferromagnet into an attached nonmagnetic metal over a macroscopic scale of several millimetres. Despite decades of research into thermoelectric materials and properties, the efficiency of thermoelectric devices has remained low due to the interdependence of the Seebeck voltage, $S$; the resistivity, $q$; and the thermal conductivity [76, 77]. One promising approach to overcome this problem and increase the versatility of thermoelectric devices involves exploiting the spin of the electron in addition to its charge and heat transport properties. In contrast to conventional thermoelectrics, this effect offers the possibility for another approach in all-solid-state energy conversion devices, since it involves properties of at least two different materials that can be optimized independently. The SSE for the laser-ablated $Fe_3O_4$ (thickness = 50 nm)//$SrTiO_3$(001) (thickness = 0.5 mm) samples was measured using the so-called longitudinal configuration. In such geometry (as shown in Figure 12(a)), a temperature gradient ($\delta T$) is applied in the $\pm z$-direction, generating a temperature difference ($\pm\delta T$) between the bottom and the top of the sample, with temperatures $T \pm \delta T$ and $T$, respectively [5].

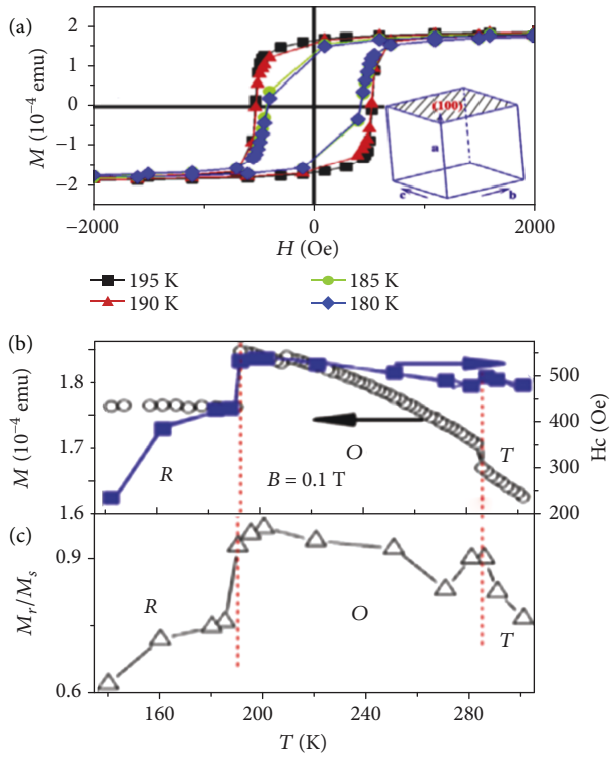


FIGURE 11: In-plane $M$-$H$ loops of $Fe_3O_4$/$BaTiO_3$ (100) heterostructures [70] measured at different temperatures (a); a variation of the in-plane magnetization vs. $T$ under a magnetic field of 0.1 T (b). The in-plane $M_r/M_s$ vs. $T$ obtained from the magnetization hysteresis loops (c).

The voltage ($V_y$) is measured along the $y$-direction, while a sweeping magnetic field is applied at an angle $h$ concerning the $x$-direction.

The focus is to observe the SSE below the Verwey transition ($T < T_V$) (Figure 12(b)), and an SSE coefficient ($S_{zy}$) at 105 K was estimated to be 52 nV/K. There is a clear reduction in SSE compared to the value observed at 300 K that could be related to the changes induced by the VT on the thermal and magnetic properties of the film, which can affect the thermal spin pumping at the $Fe_3O_4$/Pt interface and therefore the observed SSE signal. Such thermoelectric effects result from the combination between charge and heat current in suitable materials having applications as electric cooling systems or thermal power generators.

*4.3. Exchange Bias.* An exchange bias (EB) phenomenon is a property of coupled antiferromagnetic- (AFM-) ferromagnetic (FM) systems that occur due to magnetic interface effects [78]. It manifests itself in a shifting ($H_{EB}$) of $M$-$H$ loop along the field axis and enhancement of coercivity ($H_C$) when the system is cooled down in an external magnetic field through the magnetic ordering temperatures of the AFM ($T_N$) and FM ($T_C$) phases. It has been reported that the EB can be influenced by many factors in the FM/AFM system, such as the FM magnetization $M_{FM}$, the thickness of FM layer $t_{FM}$ or AFM layer $t_{AFM}$, and the anisotropy of AFM ($K_{AFM}$) or FM ($K_{FM}$) [79]. A rapid change in $K_{FM}$ is observed in the vicinity of $T_V = 120$ K due to the structural transformation from cubic to a more anisotropic monoclinic phase. Therefore, this change in $K_{FM}$ will result in variation in $H_E$. Liu et al. [6] verify this transition tunability by preparing an interface with thicknesses of $Fe_3O_4$ and CoO as 40 nm and 5 nm, respectively, in the FM/AFM bilayer system.

The FC-ZFC magnetization curves of CoO (5 nm)/$Fe_3O_4$ (40 nm)/MgO (001) AF/FM system in Figure 13(a) show a rapid change in magnetization at the VT. At the same temperature, $H_C$ observes a sharp enhancement in the AF/FM system compared to the bare $Fe_3O_4$ (40 nm)/MgO (001) layer (inset a), indicating exchange anisotropy that is coupled with magnetocrystalline anisotropy change due to structural transformation. Figure 13(b) shows notable $H_E$ change below VT. For $Fe_3O_4$, the low-temperature monoclinic magnetocrystalline anisotropy constants are considerably greater (about 10 times) than those of the high-temperature cubic structure. The correlation between $H_E{}^2$ and $H_C$ (inset b) indicates further that $K_{FM}$ has a sole responsibility for such enhancement at VT.

*4.4. Spin Accumulation.* Spin-dependent transports (particularly spin injection, manipulation, and detection) are the integral parts of semiconductor spintronic devices and have attracted tremendous attention. Recent studies have demonstrated that spin-polarized carriers injected from a ferromagnetic material to a semiconductor lead to nonequilibrium spin accumulation and spin current over spin diffusion length [80, 81]. The magnitude of spin accumulation in any system depends on factors like type of the injector, the spin polarization of the ferromagnet/insulator combination, junction resistance, and the uniformity of film at the interface. Half-metallic $Fe_3O_4$ can be a potential choice for spin injector material compared to the ferromagnetic metals.

Recently, Bhat and Kumar [7] investigated spin injection from $Fe_3O_4$ as a spin source into GaAs and Si (both $n$ and $p$-type) semiconductors using with and without a tunnel barrier (MgO) via three-terminal electrical Hanle (3TH) measurement, as shown in Figure 14(a). Application of a constant current $I$ through the $Fe_3O_4$ layer makes sure that sufficient spin-polarized carriers are pumped into the semiconductor where the decay of spin-polarized carriers will be measured. Once, the spins are injected into the semiconductor, these accumulated spin-polarized carriers at the junction of semiconductor get scattered or processed depending on the type of semiconductor. Thus, there is a gradient in the measured voltage $\Delta V$ between the device and the far end of semiconductor due to the spin-scattering process within these semiconductors which can be further controlled by applying a perpendicular magnetic field $B$. The $\Delta V$ can be expressed as $\Delta V = \text{TSP} \times \Delta\mu/2$, where TSP is the tunnel spin polarization of the ferromagnet/insulator combination and $\Delta\mu = \mu_\uparrow - \mu_\downarrow$ the difference in chemical potential for up-spins and down-spins, which is nothing but the spin accumulation at the injected material. Strikingly, the normalized spin accumulation voltage ($\Delta V/\Delta V_{max}$) (see Figure 14(b)) in the semiconductor is found to be associated with a drastic increment in $Fe_3O_4$-based devices below $T_V$. Such an enhancement of $\Delta V$ is absent in the devices with Fe as a spin

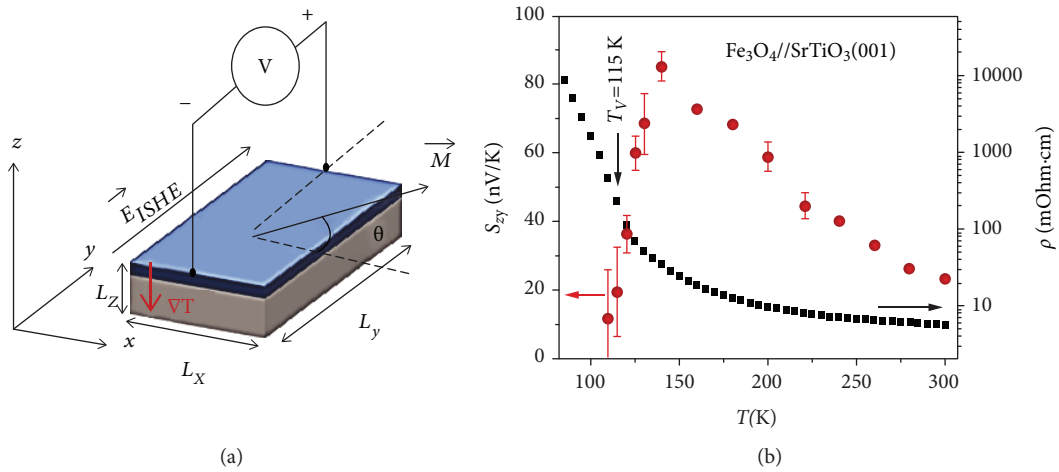


(a) (b)

Figure 12: Schematic of the measurement setup (a) and estimated SSE coefficient ($S_{zy}$) vs. $T$ (b) for the $Fe_3O_4$//$SrTiO_3$ (001) sample [5].

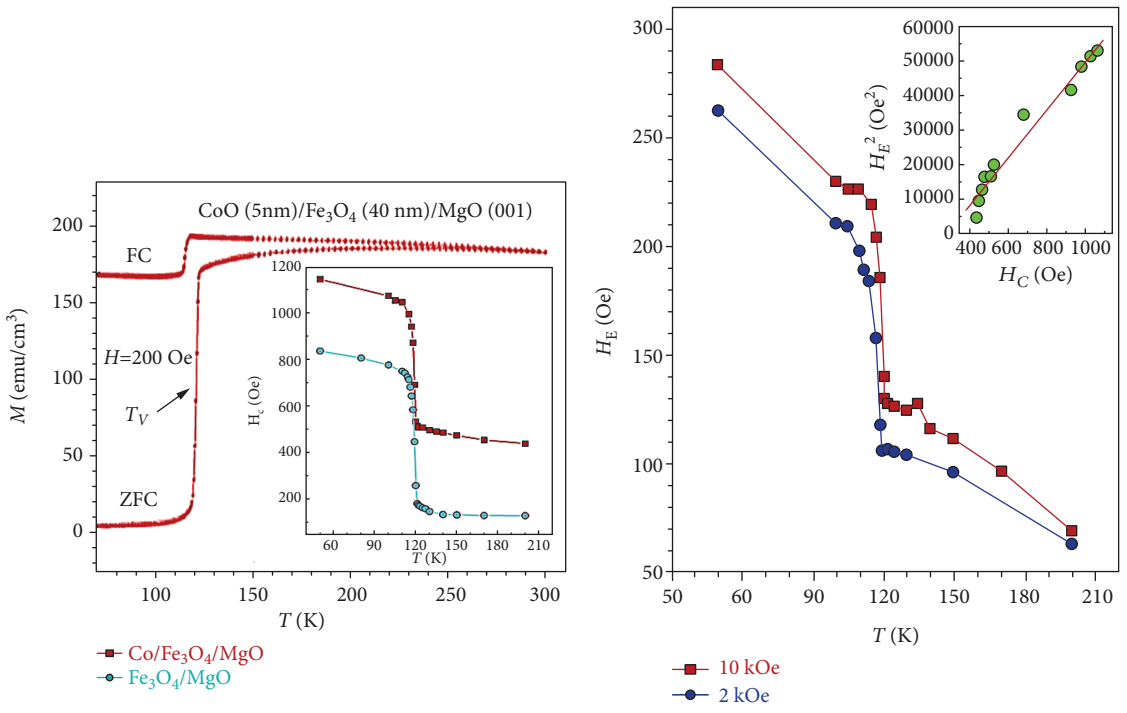


(a) (b)

Figure 13: FC-ZFC magnetization curves of CoO (5 nm)/$Fe_3O_4$ (40 nm)/MgO (001) AF/FM system (a). Inset of (a): temperature dependence of coercivity field ($H_C$) for CoO (5 nm)/$Fe_3O_4$ (40 nm)/MgO (001) and $Fe_3O_4$(40 nm)/MgO (001) systems. The exchange bias field ($H_E$) as a function of temperature at the cooling field of 10 kOe and 2 kOe (b). Inset of (b): $H_C$ vs. $H_E^2$ (right) [6].

source. Further, the overall device resistance measured by 2 probes has no drastic difference at the $T_V$ (see Figure 14(c)). From this, it can be concluded that the $T_V$ of the $Fe_3O_4$ film has a direct influence on the magnitude of spin accumulation, and the resistance enhancement of $Fe_3O_4$ film itself has no vital role in the observed enhancement of spin accumulation. This result is consistent with the investigation of Wang et al. [82] and Ziese et al. [83] showing the maximum spin polarization of $Fe_3O_4$ observed at $T_V$ using MR measurements.

Thus, an anomalous increase in $\Delta V$ can be attributed purely to the spin subband modification across $T_V$ but not to the increase in resistance. Since the VT is associated with a structural modification, the configuration of subbands of $Fe_3O_4$ along with the tunnel barrier might influence the total spin accumulation, as $\Delta V$ depends directly on the tunnel spin polarization of $Fe_3O_4$/MgO. But the similar magnitude of enhancement in spin accumulation is even present in the Schottky junction of $Fe_3O_4$ on GaAs, ruling out the role of MgO electronic band structure. Hence, the spin

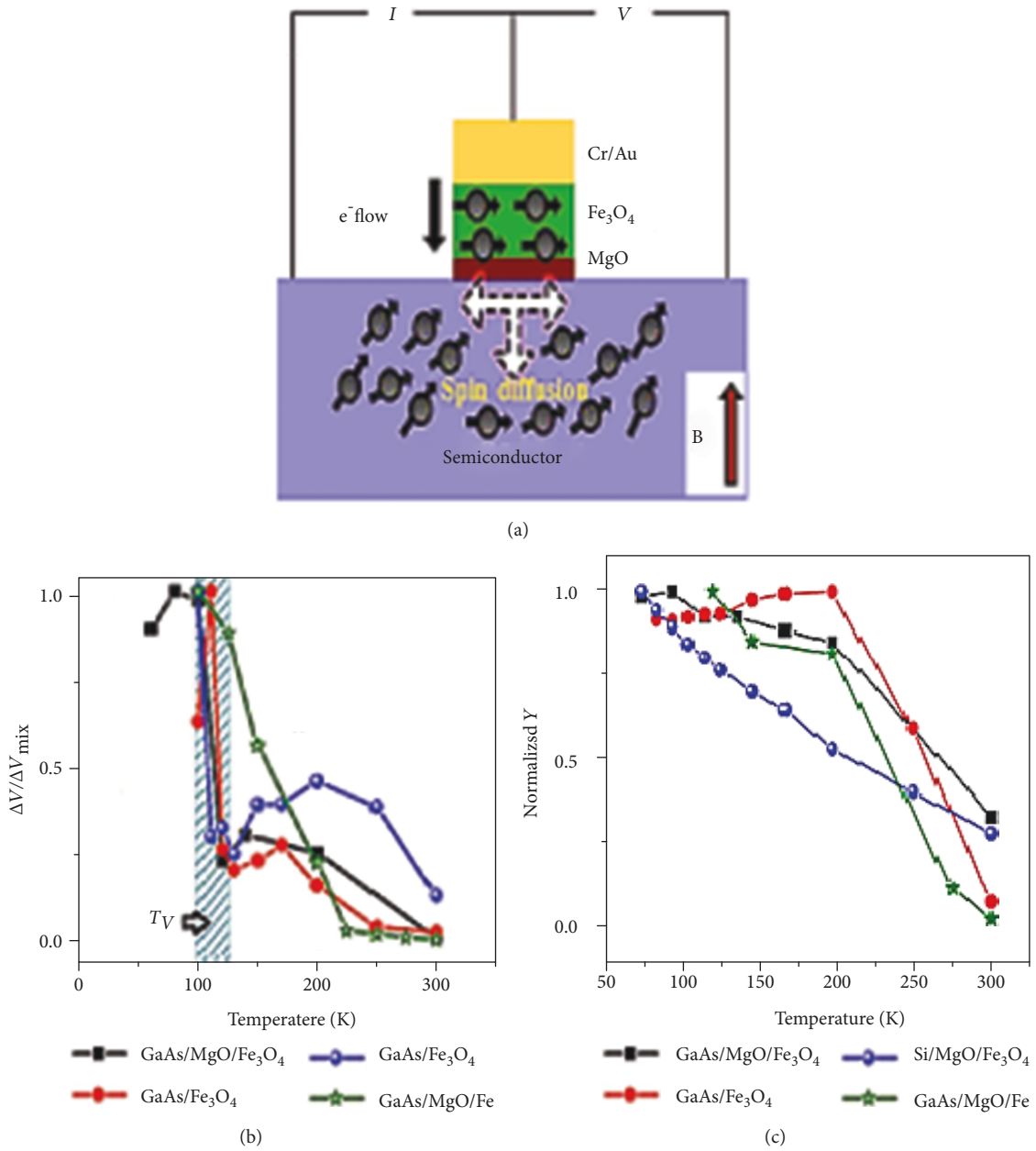


FIGURE 14: Schematics of the electrical 3TH measurement and the spin relaxation in a semiconductor (a). The plot of normalized spin accumulation voltage $\Delta V$ vs. $T$ of $Fe_3O_4$/MgO/GaAs, $Fe_3O_4$/GaAs, $Fe_3O_4$/MgO/Si, and Fe/MgO/GaAs devices showing the Verwey transition (shaded region) coinciding exactly the region of enhancement in $\Delta V$ (b) while the normalized value of local 2-probe voltages as a function of $T$ for this sample is plotted for comparison (c) [7].

injection and detection into conventional semiconductors like GaAs and Si can be improved with the help of materials like $Fe_3O_4$ with higher spin polarization. This result also suggests that the theoretical prediction of room temperature half-metallicity of $Fe_3O_4$ above and below $T_V$ has to be reinvestigated.

*4.5. Organic Spintronics.* Π-conjugated organic semiconductors (OS) are extremely attractive materials for the transport of spin-polarized electrons to long distances [84, 85]. The major difference between inorganic and organic solids is that electrical transport is via band conduction in the former and carrier hopping in the latter. The conduction (carrier/spin injection and extraction) takes place through an abstract spin valve (SV) (shown in the inset of Figure 15(c)) that filters spin-polarized electrons by alignment of the energetic position of the highest occupied molecular orbital (HOMO) or the lowest unoccupied molecular orbital (LUMO) of the OS relative to the Fermi level ($E_F$) of the ferromagnetic (FM) electrode (Figure 15(a)). This concept is applied to make memory and sensor devices working on giant magnetoresistance (GMR) and tunnel magnetoresistance (TMR). As discussed previously, $Fe_3O_4$ provides excellent spin injection at RT and supplementary spin accumulation at and below

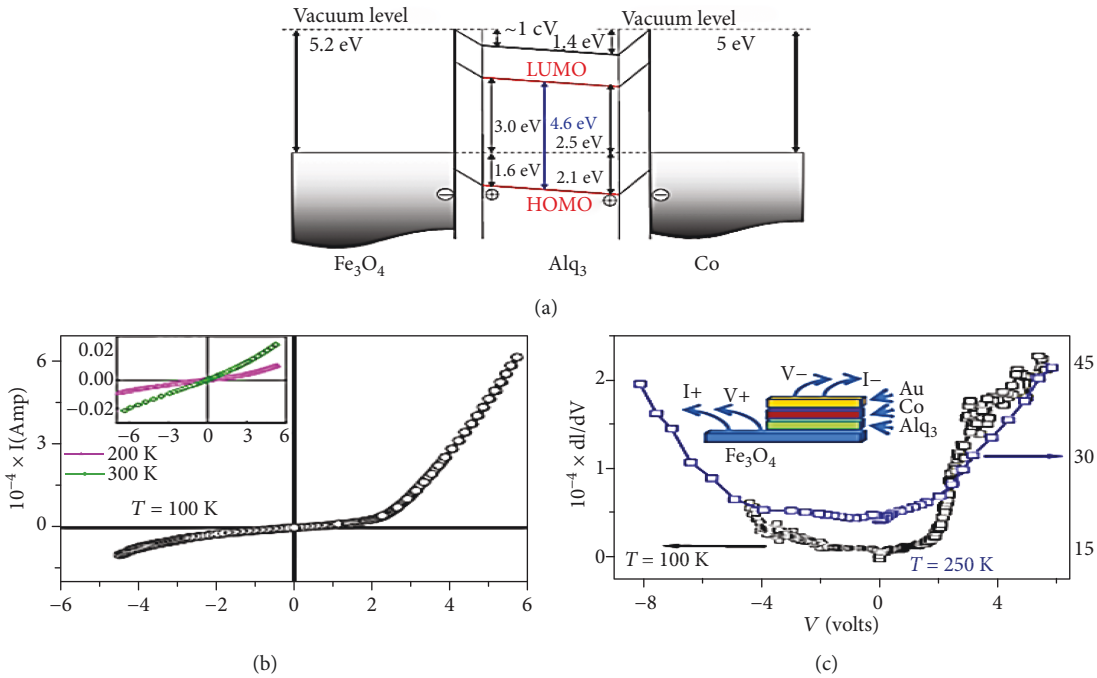


FIGURE 15: Energy level diagram at the interfaces of Alq3 and $Fe_3O_4$/Co electrodes (a). Current-voltage ($I$-$V$) characteristics of $Fe_3O_4$/Alq3/Co/Au SV at $T = 100$ K (b). Inset in (b) shows $I$-$V$ curves at $T = 200$ and 300 K. Differential conductance vs. bias voltage at $T = 100$ K and 250 K (c). Inset in (c) shows a schematic view of transport measurement geometry [84].

$T_V$ [6]. Convincingly, tuning of charge gap (0.15 eV) at $E_F$ across VT due to charge ordering on the octahedral iron sites of $Fe_3O_4$ is believed to result in a corresponding tuning of conduction mode and a unique crossover from GMR to TMR in $Fe_3O_4$/Alq3($C_{27}H_{18}N_3O_3Al$)/Co interface as proposed by Dey et al. [86] with the energy band diagram given in Figure 15(a).

Interestingly, the $I$-$V$ curves (Figure 15(b)) at higher temperatures $T > T_V$ exhibit clear signs of tunnelling which further confirms from parabolic differential d$I$/d$V$ curves (Figure 15(c)). But, at $T < T_V$, the curve is different and exhibits the beginning of the injection mode at a bias of 2 V (Figure 15(b)). The conduction observed at $T < T_V$ is described by "activated" carrier injection into the molecular orbitals of OSC at the electrode-OSC interface, followed by "activated" carrier hopping through the molecular orbitals towards the opposite electrode, where the extraction of carriers from OSC takes place. While the $T > T_V$ conduction is achieved through carrier tunnelling process, there is a drastic change in conductivity mode in SV from injection to tunnel mode as a function of "temperature," signifies VT, as the origin of this effect. For $T < T_V$, there is a formation of charge gap at $E_F$; consequently, activated carrier transport with the device current governed by carrier injection and transport through molecular levels of Alq3 could be assigned as GMR. For $T > T_V$, with the decrease or even closure of this energy gap, all the charge carriers take part in the conduction process. Activated carrier transport no more remains relevant in this scenario, and the device current should be governed by tunnelling conduction in this temperature regime. Both GMR and TMR have been observed in a single SV below/above the $T_V$, and a drastic tuning in SV properties is triggered by VT of $Fe_3O_4$ electrode.

## 5. Conclusions

The aim of current day research is to innovate electromagnetic devices with advanced materials that can operate at lower power with higher speed, yet without compromising the aim of shrinking their size. For this goal, a comprehensive review of the growth of various nanostructured $Fe_3O_4$ geometries and its hallmark Verwey transition is in a time of need. It is very exciting to observe the ensemble of anomalies VT brought forth at the nanoscale. It is not full-size dependent, but shape morphology also plays a crucial role in determining the energetically stable surface of stoichiometric $Fe_3O_4$. In nanocrystalline thin films, the electronic transport properties behave differently compared to the magnetic properties, particularly the absence of VT and the presence of antiphase boundaries caused by defects, off-stoichiometric $Fe^{2+}/Fe^{3+}$ ratio, and micro-/nanostrains emanating from different growth conditions. Interestingly, the Verwey transition temperature $T_V$ can be tailored in epitaxial $Fe_3O_4$ thin films either by compressive strain using underneath special spinel substrates or integrated with a gated circuit using the electric field.

The following are the possible applications of nanostructured $Fe_3O_4$ wherein VT can be exploited in the future:

(1) Different $Fe_3O_4$-based multiferroic heterostructures can be developed by interfacial engineering (epitaxial strain, charge, oxygen vacancy, exchange, and spin-

orbital coupling) for various novel applications like resistive switching, spin filters for data storage, and spatial light modulators for optical switching

(2) In contrast to conventional thermoelectrics, the spin Seebeck effect in $Fe_3O_4$ thin films offers new possibility in all-solid-state energy conversion devices such as electric cooling systems and thermal power generators while the observation of large magnetocaloric effect paves the way for cooler on-chip devices for nano-/microelectromechanical systems

(3) The concept of integration of $\pi$-conjugated organic semiconductors into spintronic devices owing to its robust spin coherence can be realized by using band alignment at the electrode $Fe_3O_4$/Alq3 interface, which gives GMR to TMR crossover in a single spin valve

(4) Currently, basic research is mainly focused on spin dynamics and transport in semiconductor environment (spin transistors, spin diodes, optospintronic devices, memories, etc.) for all-electrical spin control via spin-orbit interactions and fixed or mobile spin qubits for quantum computing

(5) Lastly, $Fe_3O_4$ can be convincingly used for manufacturing cheap and efficient spintronic devices because of properties like excellent spin accumulation that can be successfully controlled using the Verwey transition. It can be used in various biomedical sensors like molecular detection, e.g., protein detection, and as a potential biomarker due to its positive integration with an organic semiconductor. Microarrays of sensing devices can make use of these properties of Verwey transition in cryogenic units for electrical fault sensing

Convincingly, VT proves to be an efficient needle to tailor the fabric of $Fe_3O_4$ into useful nanoscale devices, yet shifting VT towards the room temperature range still remains a major challenge and can be manipulated by having in-depth knowledge of complicated electron-electron and electron-phonon interactions that involve the interplay of interaction, exchange orbital, and spin degrees of freedom.

## Conflicts of Interest

The authors declare that there is no conflict of interests.

## References

[1] A. Mitra, J. Mohapatra, S. S. Meena, C. V. Tomy, and M. Aslam, "Verwey transition in ultrasmall-sized octahedral $Fe_3O_4$ nanoparticles," *The Journal of Physical Chemistry C*, vol. 118, no. 33, pp. 19356–19362, 2014.

[2] S. de Jong, R. Kukreja, C. Trabant et al., "Speed limit of the insulator–metal transition in magnetite," *Nature Materials*, vol. 12, no. 10, pp. 882–886, 2013.

[3] L. R. Bickford Jr., "The low temperature transformation in ferrites," *Reviews of Modern Physics*, vol. 25, no. 1, pp. 75–79, 1953.

[4] M. Liu, J. Hoffman, J. Wang, J. Zhang, B. Nelson-Cheeseman, and A. Bhattacharya, "Non-volatile ferroelastic switching of the Verwey transition and resistivity of epitaxial $Fe_3O_4$/PMN-PT (011)," *Scientific Reports*, vol. 3, no. 1, p. 1876, 2013.

[5] R. Ramos, T. Kikkawa, K. Uchida et al., "Observation of the spin Seebeck effect in epitaxial $Fe_3O_4$ thin films," *Applied Physics Letters*, vol. 102, no. 7, article 072413, 2013.

[6] X. H. Liu, W. Liu, Z. D. Zhang, and C. F. Chang, "Mediating exchange bias by Verwey transition in CoO/$Fe_3O_4$ thin film," *Journal of Applied Physics*, vol. 123, no. 8, article 083903, 2018.

[7] S. G. Bhat and P. S. A. Kumar, "Enhanced spin accumulation in $Fe_3O_4$ based spin injection devices below the Verwey transition," *Materials Research Express*, vol. 3, no. 12, article 125905, 2016.

[8] H. Y. Huang, Z. Y. Chen, R. . P. Wang et al., "Jahn-Teller distortion driven magnetic polarons in magnetite," *Nature Communications*, vol. 8, article 15929, 2017.

[9] C. Schmitz-Antoniak, D. Schmitz, A. Warland et al., "Reversed ageing of $Fe_3O_4$ nanoparticles by hydrogen plasma," *Scientific Reports*, vol. 6, no. 1, 2016.

[10] E. Gmelin, N. Lenge, and H. Kronüller, "Specific heat of magnetite near the Verwey transition is there more than one phase transition?," *Philosophical Magazine B*, vol. 50, no. 3, pp. L41–L44, 1984.

[11] D. J. Huang, H. J. Lin, J. Okamoto et al., "Charge-orbital ordering and Verwey transition in magnetite measured by resonant soft X-ray scattering," *Physical Review Letters*, vol. 96, no. 9, 2006.

[12] T. Kim, S. Lim, and J. Hong, "Giant thermal hysteresis in Verwey transition of single domain $Fe_3O_4$ nanoparticles," *Scientific Reports*, vol. 8, no. 5092, 2018.

[13] J. A. Cuenca, K. Bugler, S. Taylor et al., "Study of the magnetite to maghemite transition using microwave permittivity and permeability measurements," *Journal of Physics: Condensed Matter*, vol. 28, no. 10, article 106002, 2016.

[14] M. A. Gilleo, "Superexchange interaction energy for $Fe^{3+}$-$O^{2-}$-$Fe^{3+}$ linkages," *Physical Review*, vol. 109, no. 3, pp. 777–781, 1958.

[15] C. Zener, "Interaction between the *d*-shells in the transition metals. II. Ferromagnetic compounds of manganese with perovskite structure," *Physical Review*, vol. 82, no. 3, pp. 403–405, 1951.

[16] E. J. W. Verwey and P. W. Haayman, "Electronic conductivity and transition point of magnetite ("$Fe_3O_4$")," *Physica*, vol. 8, no. 9, pp. 979–987, 1941.

[17] Z. Tarnawski, A. Wiecheć, M. Madej et al., "Studies of the Verwey transition in magnetite," *Acta Physica Polonica A*, vol. 106, no. 5, pp. 771–775, 2004.

[18] A. Kozłowski, Z. Kąkol, and Z. Tarnawski, "Magnetite $Fe_3O_4$: the correlated electron-phonon system," *Acta Physica Polonica A*, vol. 111, no. 4, pp. 537–547, 2007.

[19] S. Lim, B. Choi, S. Y. Lee et al., "Microscopic states and the Verwey transition of magnetite nanocrystals investigated by nuclear magnetic resonance," *Nano Letters*, vol. 18, no. 3, pp. 1745–1750, 2018.

[20] J. Lee, S. G. Kwon, J.-G. Park, and T. Hyeon, "Size dependence of metal–insulator transition in stoichiometric

$Fe_3O_4$ nanocrystals," *Nano Letters*, vol. 15, no. 7, pp. 4337–4342, 2015.

[21] A. Akbarzadeh, M. Samiei, and S. Davaran, "Magnetic nanoparticles: preparation, physical properties, and applications in biomedicine," *Nanoscale Research Letters*, vol. 7, no. 1, p. 144, 2012.

[22] Z. L. Lu, M. X. Xu, W. Q. Zou et al., "Large low field magnetoresistance in ultrathin nanocrystalline magnetite $Fe_3O_4$ films at room temperature," *Applied Physics Letters*, vol. 91, no. 10, article 102508, 2007.

[23] R. Aragon, P. M. Gehring, and S. M. Shapiro, "Stoichiometry, percolation, and Verwey ordering in magnetite," *Physical Review Letters*, vol. 70, no. 11, pp. 1635–1638, 1993.

[24] V. A. M. Brabers, F. Walz, and H. Kronmuller, "Impurity effects upon the Verwey transition in magnetite," *Physical Review B*, vol. 58, no. 21, pp. 14163–14166, 1998.

[25] X. H. Liu, A. D. Rata, C. F. Chang, A. C. Komarek, and L. H. Tjeng, "Verwey transition in $Fe_3O_4$ thin films: influence of oxygen stoichiometry and substrate-induced microstructure," *Physical Review B*, vol. 90, no. 12, article 125142, 2014.

[26] M. Bohra, K. E. Prasad, R. Bollina, S. C. Sahoo, and N. Kumar, "Characterizing the phase purity of nanocrystalline $Fe_3O_4$ thin films using Verwey transition," *Journal of Magnetism and Magnetic Materials*, vol. 418, pp. 137–142, 2016.

[27] M. Bohra, S. Prasad, N. Venketaramani, N. Kumar, S. C. Sahoo, and R. Krishnan, "Magnetic properties of magnetite thin films close to the Verwey transition," *Journal of Magnetism and Magnetic Materials*, vol. 321, no. 22, pp. 3738–3741, 2009.

[28] M. Bohra, D. Roy Chowdhury, J.-F. Bobo, and V. Singh, "Anomalous electric transport across Verwey transition in nanocrystalline $Fe_3O_4$ thin films," *Journal of Applied Physics*, vol. 125, no. 1, article 013901.

[29] M. Bohra and S. C. Sahoo, "Large magnetocaloric effect at Verwey point in nanocrystalline $Fe_3O_4$ thin films," *Journal of Alloys and Compounds*, vol. 699, pp. 1118–1121, 2017.

[30] X. Liu, C.-F. Chang, A. D. Rata, A. C. Komarek, and L. H. Tjeng, "$Fe_3O_4$ thin films: controlling and manipulating an elusive quantum material," *npj Quantum Materials*, vol. 1, no. 1, article 16027, 2016.

[31] M. Ziese, "Extrinsic magnetotransport phenomena in ferromagnetic oxides," *Reports on Progress in Physics*, vol. 65, no. 2, pp. 143–249, 2002.

[32] J. B. Moussy, "From epitaxial growth of ferrite thin films to spin-polarized tunnelling," *Journal of Physics D: Applied Physics*, vol. 46, no. 14, article 143001, 2013.

[33] G. Q. Gong, A. Gupta, G. Xiao, W. Qian, and V. P. Dravid, "Magnetoresistance and magnetic properties of epitaxial magnetite thin films," *Physical Review B*, vol. 56, no. 9, pp. 5096–5099, 1997.

[34] S. Geprägs, D. Mannix, M. Opel, S. T. B. Goennenwein, and R. Gross, "Converse magnetoelectric effects in $Fe_3O_4/BaTiO_3$ multiferroic hybrids," *Physical Review B*, vol. 88, no. 5, article 054412, 2013.

[35] W. Eerenstein, T. T. M. Palstra, T. Hibma, and S. Celotto, "Origin of the increased resistivity in epitaxial $Fe_3O_4$ films," *Physical Review B*, vol. 66, no. 20, article 201101, 2002.

[36] X. Liu, W. Mi, Q. Zhang, and X. Zhang, "Anisotropic magnetoresistance across Verwey transition in charge ordered $Fe_3O_4$ epitaxial films," *Physical Review B*, vol. 96, no. 21, article 214434, 2017.

[37] S. Chandra, R. Das, V. Kalappattil et al., "Epitaxial magnetite nanorods with enhanced room temperature magnetic anisotropy," *Nanoscale*, vol. 9, no. 23, pp. 7858–7867, 2017.

[38] A. Lak, D. Niculaes, G. C. Anyfantis et al., "Facile transformation of $FeO/Fe_3O_4$ core-shell nanocubes to $Fe_3O_4$ via magnetic stimulation," *Scientific Reports*, vol. 6, no. 1, article 33295, 2016.

[39] G. T. Rado and J. M. Ferrari, "Electric field dependence of the magnetic anisotropy energy in magnetite ($Fe_3O_4$)," *Physical Review B*, vol. 12, no. 11, pp. 5166–5174, 1975.

[40] S. Iida, M. Mizoguchi, S. Umemura, J. Yoshida, K. Kato, and K. Yanai, "Typical spontaneous symmetry breakdown in solid state as revealed by Fe3O4," *Journal of Applied Physics*, vol. 50, no. B11, p. 7584, 1979.

[41] G. T. Rado and J. M. Ferrari, "Linear and bilinear magnetoelectric effects in magnetically biased magnetite ($Fe_3O_4$)," *Physical Review B*, vol. 15, no. 1, pp. 290–297, 1977.

[42] Y. Miyamoto and S. Chikazumi, "Crystal symmetry of magnetite in low temperature phase deduced from magnetoelectric measurements," *Journal of the Physical Society of Japan*, vol. 57, no. 6, pp. 2040–2050, 1988.

[43] Y. Miyamoto and M. Shindo, "Magnetoelectric measurement of magnetite ($Fe_3O_4$) at low temperatures and direct evidence for nonexistence of *ac* mirror plane," *Journal of the Physical Society of Japan*, vol. 62, no. 5, pp. 1423–1426, 1993.

[44] Y. Miyamoto, S. Ishihara, T. Hirano, M. Takada, and N. Suzuki, "Ferroelectricity of magnetite ($Fe_3O_4$) observed by means of magnetoelectric effect," *Solid State Communications*, vol. 89, no. 1, pp. 51–54, 1994.

[45] L. Pauling, "The structure and entropy of ice and of other crystals with some randomness of atomic arrangement," *Journal of the American Chemical Society*, vol. 57, no. 12, pp. 2680–2684, 1935.

[46] L. Pauling, *The Nature of the Chemical Bond*, Cornel University Press, Ithaca, NY, USA, 1938.

[47] J. P. Wright, J. P. Attfield, and P. G. Radaelli, "Long range charge ordering in magnetite below the Verwey transition," *Physical Review Letters*, vol. 87, no. 26, article 266401, 2001.

[48] J. P. Wright, J. P. Attfield, and P. G. Radaelli, "Charge ordered structure of magnetite Fe3O4 below the Verwey transition," *Physical Review B*, vol. 66, no. 21, article 214422, 2002.

[49] J. van den Brink and D. I. Khomskii, "Multiferroicity due to charge ordering," *Journal of Physics: Condensed Matter*, vol. 20, no. 43, article 434217, 2008.

[50] M. Ziese, P. D. Esquinazi, D. Pantel, M. Alexe, N. M. Nemes, and M. Garcia-Hernández, "Magnetite ($Fe_3O_4$): a new variant of relaxor multiferroic?," *Journal of Physics: Condensed Matter*, vol. 24, no. 8, article 086007, 2012.

[51] J. J. I. Wong, A. G. Swartz, R. Zheng, W. Han, and R. K. Kawakami, "Electric field control of the Verwey transition and induced magnetoelectric effect in magnetite," *Physical Review B*, vol. 86, no. 6, article 060409, 2012.

[52] K. Yamauchi, T. Fukushima, and S. Picozzi, "Ferroelectricity in multiferroic magnetite $Fe_3O_4$ driven by noncentrosymmetric $Fe^{2+/}Fe^{3+}$ charge-ordering: first-principles study," *Physical Review B*, vol. 79, no. 21, article 212404, 2009.

[53] F. Walz and H. Kronmüller, "Analysis of magnetic point-defect relaxations in electron-irradiated magnetite," *Physica Status Solidi B*, vol. 181, no. 2, pp. 485–498, 1994.

[54] F. Schrettle, S. Krohns, P. Lunkenheimer, V. A. M. Brabers, and A. Loidl, "Relaxor ferroelectricity and the freezing of short-range polar order in magnetite," *Physical Review B*, vol. 83, no. 19, article 195109, 2011.

[55] V. Chlan, K. Kouřil, H. Štěpánková et al., "Magnetically induced structural reorientation in magnetite studied by nuclear magnetic resonance," *Journal of Applied Physics*, vol. 108, no. 8, article 083914, 2010.

[56] L. E. Cross, "Relaxor ferroelectrics," *Ferroelectrics*, vol. 76, no. 1, pp. 241–267, 1987.

[57] Y. Tokura, "Multiferroics—toward strong coupling between magnetization and polarization in a solid," *Journal of Magnetism and Magnetic Materials*, vol. 310, no. 2, pp. 1145–1150, 2007.

[58] I. E. Dzyaloshinskii, "On the magneto-electrical effects in antiferromagnets," *Soviet Physics JETP*, vol. 10, pp. 628-629, 1960.

[59] M. K. Niranjan, J. P. Velev, C.-G. Duan, S. S. Jaswal, and E. Y. Tsymbal, "Magnetoelectric effect at the $Fe_3O_4/BaTiO_3$ (001) interface: a first-principles study," *Physical Review B*, vol. 78, no. 10, article 104405, 2008.

[60] Y. Zhang, M. Liu, L. Zhang et al., "Multiferroic heterostructures of $Fe_3O_4$/PMN-PT prepared by atomic layer deposition for enhanced interfacial magnetoelectric couplings," *Applied Physics Letters*, vol. 110, no. 8, article 082902, 2017.

[61] I. Vrejoiu, D. Preziosi, A. Morelli, and E. Pippel, "Multiferroic $PbZr_xTi_{1-x}O_3/Fe_3O_4$ epitaxial sub-micron sized structures," *Applied Physics Letters*, vol. 100, no. 10, article 102903, 2012.

[62] J. Wang, J. B. Neaton, H. Zheng et al., "Epitaxial $BiFeO_3$ multiferroic thin film heterostructures," *Science*, vol. 299, no. 5613, pp. 1719–1722, 2003.

[63] H. W. Brinks, H. Fjellvag, and A. Kjekshus, "Synthesis of metastable perovskite-type $YMnO_3$ and $HoMnO_3$," *Journal of Solid State Chemistry*, vol. 129, no. 2, pp. 334–340, 1997.

[64] Y.-M. Kim, A. Morozovska, E. Eliseev et al., "Direct observation of ferroelectric field effect and vacancy-controlled screening at the $BiFeO_3/La_xSr_{1-x}MnO_3$ interface," *Nature Materials*, vol. 13, no. 11, pp. 1019–1025, 2014.

[65] C. Becher, M. Trassin, M. Lilienblum et al., "Functional ferroic heterostructures with tunable integral symmetry," *Nature Communications*, vol. 5, no. 1, p. 4295, 2014.

[66] W. Saenrang, B. A. Davidson, F. Maccherozzi et al., "Deterministic and robust room-temperature exchange coupling in monodomain multiferroic $BiFeO_3$ heterostructures," *Nature Communications*, vol. 8, no. 1, p. 1583, 2017.

[67] G. De Luca, N. Strkalj, S. Manz, C. Bouillet, M. Fiebig, and M. Trassin, "Nanoscale design of polarization in ultrathin ferroelectric heterostructures," *Nature Communications*, vol. 8, no. 1, p. 1419, 2017.

[68] Y. Zhang, L. Xie, J. Kim et al., "Discovery of a magnetic conductive interface in $PbZr_{0.2}Ti_{0.8}O_3/SrTiO_3$ heterostructures," *Nature Communications*, vol. 9, no. 1, p. 685, 2018.

[69] C. Ju, J.-C. Yang, C. Luo et al., "Anomalous electronic anisotropy triggered by ferroelastic coupling in multiferroic heterostructures," *Advanced Materials*, vol. 28, no. 5, pp. 876–883, 2016.

[70] H. F. Tian, T. L. Qu, L. B. Luo et al., "Strain induced magnetoelectric coupling between magnetite and $BaTiO_3$," *Applied Physics Letters*, vol. 92, no. 6, article 063507, 2008.

[71] Z. Yang, C. Ko, and S. Ramanathan, "Oxide electronics utilizing ultrafast metal-insulator transitions," *Annual Review of Materials Research*, vol. 41, no. 1, pp. 337–367, 2011.

[72] T. N. Theis and P. M. Solomon, "It's time to reinvent the transistor!," *Science*, vol. 327, no. 5973, pp. 1600-1601, 2010.

[73] C. H. Ahn, J. M. Triscone, and J. Mannhart, "Electric field effect in correlated oxide systems," *Nature*, vol. 424, no. 6952, pp. 1015–1018, 2003.

[74] T. Kopp and J. Mannhart, "Calculation of the capacitances of conductors: perspectives for the optimization of electronic devices," *Journal of Applied Physics*, vol. 106, no. 6, article 064504, 2009.

[75] R. Scherwitzl, P. Zubko, I. G. Lezama et al., "Electric-field control of the metal-insulator transition in ultrathin $NdNiO_3$ films," *Advanced Materials*, vol. 22, no. 48, pp. 5517–5520, 2010.

[76] J. P. Heremans, V. Jovovic, E. S. Toberer et al., "Enhancement of thermoelectric efficiency in PbTe by distortion of the electronic density of states," *Science*, vol. 321, no. 5888, pp. 554–557, 2008.

[77] H. Jin, C. M. Jaworski, and J. P. Heremans, "Enhancement in the figure of merit of p-type $Bi_{100-x}Sb_x$ alloys through multiple valence-band doping," *Applied Physics Letters*, vol. 101, no. 5, article 053904, 2012.

[78] W. H. Meiklejohn and C. P. Bean, "New magnetic anisotropy," *Physical Review*, vol. 102, no. 5, pp. 1413-1414, 1956.

[79] X. H. Liu, W. Liu, S. Guo, W. J. Gong, J. N. Feng, and Z. D. Zhang, "Strong effects of magnetic anisotropy on exchange coupling and magnetotransport properties of ferromagnetic/NiO/ferromagnetic trilayers," *Applied Physics Letters*, vol. 97, no. 7, article 072502, 2010.

[80] C. H. Li, O. M. J. van 't Erve, and B. T. Jonker, "Electrical injection and detection of spin accumulation in silicon at 500 K with magnetic metal/silicon dioxide contacts," *Nature Communications*, vol. 2, no. 1, p. 245, 2011.

[81] H. Saito, S. Watanabe, Y. Mineno et al., "Electrical creation of spin accumulation *p*-type germanium," *Solid State Communications*, vol. 151, no. 17, pp. 1159–1161, 2011.

[82] W. Wang, M. Yu, M. Batzill, J. He, U. Diebold, and J. Tang, "Enhanced tunneling magnetoresistance and high-spin polarization at room temperature in a polystyrene-coated $Fe_3O_4$ granular system," *Physical Review B*, vol. 73, no. 13, article 134412, 2006.

[83] M. Ziese, U. Köhler, A. Bollero, R. Höhne, and P. Esquinazi, "Schottky barrier and spin polarization at the $Fe_3O_4$–Nb:$SrTiO_3$ interface," *Physical Review B*, vol. 71, no. 18, article 180406, 2005.

[84] G. Schmidt, D. Ferrand, L. W. Molenkamp, A. T. Filip, and B. J. van Wees, "Fundamental obstacle for electrical spin injection from a ferromagnetic metal into a diffusive semiconductor," *Physical Review B*, vol. 62, no. 8, pp. R4790–R4793, 2000.

[85] J. S. Moodera, L. R. Kinder, T. M. Wong, and R. Meservey, "Large magnetoresistance at room temperature in ferromagnetic thin film tunnel junctions," *Physical Review Letters*, vol. 74, no. 16, pp. 3273–3276, 1995.

[86] P. Dey, R. Rawat, S. R. Potdar, R. J. Choudhary, and A. Banerjee, "Temperature driven transition from giant to tunneling magneto-resistance in $Fe_3O_4$/Alq3/Co spin valve: role of Verwey transition of $Fe_3O_4$," *Journal of Applied Physics*, vol. 115, no. 17, article 17C110, 2014.